
An OpenGL and C++ based function library for curve and surface modeling in a large class of extended Chebyshev spaces

Ágoston Róth

Submitted to arXiv on August 15, 2017

Abstract Applying original and existing theoretical results, we propose a platform-independent multi-threaded function library that provides data structures to generate, differentiate and render both the ordinary basis and the non-negative normalized B-basis of an arbitrary extended Chebyshev (EC) space that comprises the constants and can be identified with the solution space of a user-defined constant-coefficient homogeneous linear differential equation. Using the obtained non-negative normalized B-bases, our library can also generate, (partially) differentiate, modify and visualize a large family of so-called B-curves and tensor product B-surfaces. Moreover, the library also implements methods that can be used to perform general order elevation, to subdivide B-curves and B-surfaces by means of general de Casteljau-like B-algorithms, and to generate general basis transformations for the control point based exact description of arbitrary integral curves and surfaces that are described in traditional parametric form by means of the ordinary bases of the underlying EC spaces. Independently of the algebraic, exponential, trigonometric or mixed type of the applied EC space, the proposed library is numerically stable and efficient up to a reasonable dimension number and may be useful for academics and engineers in the fields of Approximation Theory, Computer Aided Geometric Design, Computer Graphics, Isogeometric and Numerical Analysis.

Keywords extended Chebyshev spaces · constant-coefficient homogeneous linear differential equations · non-negative normalized B-basis · B-curve/surface modeling · order (dimension) elevation · subdivision (B-algorithm) · basis transformation · control point based exact description · OpenGL · OpenMP

Mathematics Subject Classification (2000) 65D17 · 68U07

1 Introduction

The following subsections detail our motivations, main objectives and the structure of the manuscript.

1.1 Motivations

Non-negative normalized B-bases (a comprehensive study of which can be found in [17] and references therein) are normalized totally positive bases that imply optimal shape preserving properties for the representation of curves described as linear combinations of control points and basis functions. Considering a non-empty compact definition domain $[\alpha, \beta] \subset \mathbb{R}$, the most well-known representative of such bases are the classical Bernstein polynomials of degree $n \in \mathbb{N}$, cf. [4]. Similarly to them, non-negative normalized B-bases provide shape preserving properties like closure for the affine transformations of the control polygon, convex hull, variation diminishing (which also implies convexity preserving of plane control polygons), endpoint interpolation, monotonicity preserving, hodograph and length diminishing, and a recursive corner cutting algorithm (also called B-algorithm) that is the analogue of the de Casteljau algorithm of classical Bézier curves. Among all normalized totally positive bases of a given vector space of functions a normalized B-basis is the least variation diminishing and the shape of the generated curve more mimics its control polygon. Important curve design algorithms like evaluation, subdivision, degree (or dimension) elevation or knot insertion are in fact corner cutting algorithms that can be treated in a unified way by means of B-algorithms induced by B-bases.

This research was supported by the European Union and the State of Hungary, co-financed by the European Social Fund in the framework of TÁMOP-4.2.4.A/2-11/1-2012-0001 'National Excellence Program'.

Á. Róth

Department of Mathematics and Computer Science of the Hungarian Line, Babeş-Bolyai University, RO-400084 Cluj-Napoca, Romania

Tel.: +40-264-405300

Fax: +40-264-591906

E-mail: agoston_roth@yahoo.com



Curve and surface modeling tools based on non-polynomial non-negative normalized B-bases also ensure further advantages like: possible shape or design parameters; singularity free exact parametrization (e.g. parametrization of conic sections may correspond to natural arc-length parametrization); higher or even infinite order of precision concerning (partial) derivatives; ordinary (i.e., traditionally parametrized) integral curves and surfaces can be described exactly by means of control points without any additional weights (the calculation of which, apart from some simple cases, is cumbersome for the designer); important transcendental curves and surfaces which are of interest in real-life applications can also be represented exactly (the standard rational Bézier or NURBS models cannot encompass these geometric objects). Moreover, concerning condition numbers and stability, a non-negative normalized B-basis is the unique normalized totally positive basis that is optimally stable among all non-negative bases of a given vector space of functions, cf. [17, Corollary 3.4, p. 89].

Apart from their interest in the classical contexts of Computer Aided Geometric Design, Numerical Analysis and Approximation Theory, non-negative normalized B-bases and their spline counterparts have also been used in Isogeometric Analysis recently (consider e.g. [14] and references therein). Compared with classical finite element methods, Isogeometric Analysis provides several advantages when one describes the geometry by generalized B-splines and invokes an isoparametric approach in order to approximate the unknown solutions of differential equations (e.g. of Poisson type problems) or Dirichlet boundary conditions by the same type of functions.

These advantageous properties make non-negative normalized B-bases ideal blending function system candidates for curve and surface modeling.

1.2 Objectives

In order to be able to formulate the main objectives of the manuscript, we will use the following well-known notions. Let $n \geq 1$ be a fixed integer and consider the extended Chebyshev (EC) system

$$\mathcal{F}_n^{\alpha,\beta} = \{\varphi_{n,i}(u) : u \in [\alpha, \beta]\}_{i=0}^n, \quad \varphi_{n,0} \equiv 1, \quad -\infty < \alpha < \beta < \infty \quad (1)$$

of basis functions in $C^n([\alpha, \beta])$, i.e., by definition [8], for any integer $0 \leq r \leq n$, any strictly increasing sequence of knot values $\alpha \leq u_0 < u_1 < \dots < u_r \leq \beta$, any positive integers (or multiplicities) $\{m_k\}_{k=0}^r$ such that $\sum_{k=0}^r m_k = n + 1$, and any real numbers $\{\xi_{k,\ell}\}_{k=0, \ell=0}^{r, m_k-1}$ there always exists a unique function

$$f := \sum_{i=0}^n \lambda_{n,i} \varphi_{n,i} \in \mathbb{S}_n^{\alpha,\beta} := \langle \mathcal{F}_n^{\alpha,\beta} \rangle := \text{span } \mathcal{F}_n^{\alpha,\beta}, \quad \lambda_{n,i} \in \mathbb{R}, \quad i = 0, 1, \dots, n \quad (2)$$

that satisfies the conditions of the Hermite interpolation problem

$$f^{(\ell)}(u_k) = \xi_{k,\ell}, \quad \ell = 0, 1, \dots, m_k - 1, \quad k = 0, 1, \dots, r. \quad (3)$$

In what follows, we assume that the sign-regular determinant of the coefficient matrix of the linear system (3) of equations is strictly positive for any permissible parameter settings introduced above. Under these circumstances, the vector space $\mathbb{S}_n^{\alpha,\beta}$ of functions is called an EC space of dimension $n + 1$. In terms of zeros, this definition means that any non-zero element of $\mathbb{S}_n^{\alpha,\beta}$ vanishes at most n times in the interval $[\alpha, \beta]$. Such spaces and their corresponding spline counterparts have been widely studied, consider e.g. articles [1, 2, 5, 7, 9–13, 15, 16, 19, 20] and many other references therein.

Hereafter we will also refer to $\mathcal{F}_n^{\alpha,\beta}$ as the ordinary basis of $\mathbb{S}_n^{\alpha,\beta}$. Using [6, Theorem 5.1] it follows that the vector space $\mathbb{S}_n^{\alpha,\beta}$ also has a strictly totally positive basis, i.e., a basis such that all minors of all its collocation matrices are strictly positive. Since the constant function $1 \equiv \varphi_{n,0} \in \mathbb{S}_n^{\alpha,\beta}$, the aforementioned strictly positive basis is normalizable, therefore the vector space $\mathbb{S}_n^{\alpha,\beta}$ also has a unique non-negative normalized B-basis

$$\mathcal{B}_n^{\alpha,\beta} = \{b_{n,i}(u) : u \in [\alpha, \beta]\}_{i=0}^n \quad (4)$$

that apart from the identity

$$\sum_{i=0}^n b_{n,i}(u) \equiv 1, \quad \forall u \in [\alpha, \beta] \quad (5)$$

also fulfills the properties

$$b_{n,0}(\alpha) = b_{n,n}(\beta) = 1, \quad (6)$$

$$b_{n,i}^{(j)}(\alpha) = 0, \quad j = 0, \dots, i-1, \quad b_{n,i}^{(i)}(\alpha) > 0, \quad (7)$$

$$b_{n,i}^{(j)}(\beta) = 0, \quad j = 0, 1, \dots, n-1-i, \quad (-1)^{n-i} b_{n,i}^{(n-i)}(\beta) > 0 \quad (8)$$

conform [6, Theorem 5.1] and [15, Equation (3.6)]. (In order to avoid ambiguity, in case of some figures we will also use the notation $\overline{\mathcal{F}}_n^{\alpha,\beta}$ instead of $\mathcal{B}_n^{\alpha,\beta}$.)



All algorithms that will be presented in the forthcoming sections are valid in case of any EC space of type $\mathbb{S}_n^{\alpha,\beta}$, however in case of their C++ and OpenGL based implementation we always assume that $\mathbb{S}_n^{\alpha,\beta}$ can be identified with the solution space of the constant-coefficient homogeneous linear differential equation

$$\sum_{i=0}^{n+1} \gamma_i v^{(i)}(u) = 0, \quad \gamma_i \in \mathbb{R}, \quad u \in [\alpha, \beta] \quad (9)$$

of order $n+1$. Such a solution space is translation invariant and it is spanned by those ordinary basis functions that are generated by the (higher order) zeros of the characteristic polynomial

$$p_{n+1}(z) = \sum_{i=0}^{n+1} \gamma_i z^i, \quad z \in \mathbb{C} \quad (10)$$

associated with the differential equation (9). In order to ensure that $\varphi_{n,0} \equiv 1 \in \mathbb{S}_n^{\alpha,\beta}$, we will assume that $z=0$ is at least a first order zero of the characteristic polynomial (10). As we will see, the proposed algorithms do not assume that (10) is an either odd or even function, but if this the case, the underlying EC space will also be reflection invariant. For example, if $\{\omega_k\}_{k=1}^n$ are pairwise distinct non-zero real numbers and the length of the definition domain $[\alpha, \beta]$ is appropriately fixed, then in case of the characteristic polynomials

$$p_{n+1}(z) = z^{n+1}, \quad p_{(n+1)^2}(z) = z^{n+1} \prod_{k=1}^n (z^2 + \omega_k^2)^{n+1-k} \quad \text{and} \quad p_{(n+1)^2}(z) = z^{n+1} \prod_{k=1}^n (z^2 - \omega_k^2)^{n+1-k}$$

the corresponding pure polynomial, mixed algebraic-trigonometric and mixed algebraic-hyperbolic EC spaces

$$\begin{aligned} \mathbb{P}_n^{\alpha,\beta} &:= \left\langle \mathcal{P}_n^{\alpha,\beta} \right\rangle := \left\langle \{1, u, \dots, u^n : u \in [\alpha, \beta]\} \right\rangle, \quad \dim \mathbb{P}_n^{\alpha,\beta} = n+1, \\ \mathbb{AT}_{n(n+2)}^{\alpha,\beta} &:= \left\langle \mathcal{P}_n^{\alpha,\beta} \cup \left\{ u^\ell \cos(\omega_k u), u^\ell \sin(\omega_k u) : u \in [\alpha, \beta] \right\}_{k=1, \ell=0}^{n, n-k} \right\rangle, \quad \dim \mathbb{AT}_{n(n+2)}^{\alpha,\beta} = (n+1)^2, \end{aligned}$$

and

$$\mathbb{AH}_{n(n+2)}^{\alpha,\beta} := \left\langle \mathcal{P}_n^{\alpha,\beta} \cup \left\{ u^\ell \cosh(\omega_k u), u^\ell \sinh(\omega_k u) : u \in [\alpha, \beta] \right\}_{k=1, \ell=0}^{n, n-k} \right\rangle, \quad \dim \mathbb{AH}_{n(n+2)}^{\alpha,\beta} = (n+1)^2,$$

respectively, are translation and reflection invariant and also possess unique non-negative normalized B-basis functions. As special cases, the EC vector spaces of pure trigonometric and hyperbolic polynomials of order at most n (or of degree at most $2n$) would correspond to the characteristic polynomials

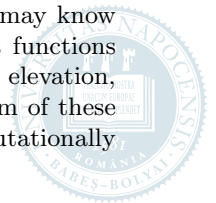
$$p_{2n+1}(z) = z \prod_{k=1}^n (z^2 + k^2) \quad \text{and} \quad p_{2n+1}(z) = z \prod_{k=1}^n (z^2 - k^2),$$

respectively, i.e., $\omega_k = k$ for all $k = 1, \dots, n$.

Based on both original and existing theoretical results, the main objective of the manuscript is to propose and implement general algorithms into a robust and flexible OpenGL and C++ based multi-threaded function library that can be used:

- to automatically generate and evaluate the derivatives of any order of both the ordinary basis and the non-negative normalized B-basis of a not necessarily reflection invariant EC space that can be identified with the translation invariant solution space of the differential equation (9);
- to describe, generate, manipulate and render so-called EC B-curves defined as convex combinations of control points and non-negative normalized B-basis functions;
- to generate, manipulate and render so-called EC B-surfaces defined as tensor products of EC B-curves;
- to elevate the dimension of the underlying EC space(s) and consequently the order(s) of the EC B-curve (surface) that is rendered;
- to subdivide EC B-curves by means of general B-algorithms implied by the non-negative normalized B-basis of the given EC space and to extend this subdivision technique to EC B-surfaces;
- to generate transformations matrices that map the non-negative normalized B-bases of the applied EC spaces to their ordinary bases, in order to ensure control point configurations for the exact description of large classes of integral curves and surfaces that are described in traditional parametric form by means of the ordinary bases of the used EC spaces.

During our study, we will also investigate the correctness and computational complexity of the proposed algorithms. To the best of our knowledge, such a general framework was not presented in the literature. Naturally, in certain special cases (like in EC spaces of pure traditional, trigonometric and hyperbolic polynomials of finite degree) one may provide more efficient curve and surface modeling techniques, since one may know the explicit expressions or other useful properties of the applied non-negative normalized B-basis functions that may lead to numerically more stable and efficient algorithms related to differentiation, order elevation, subdivision and basis transformations. However, in general, one does not even know the closed form of these ideal basis functions (e.g. they may appear in integral [12] or in determinant form [15] that are computationally



difficult and expensive to evaluate either by hand, or by numerical methods). Therefore, one has to make a compromise between a robust flexible design possibility that can be universally applied in a more general context and another special modeling technique that may be more efficient but it was developed for the solution of a very special design problem.

As we will see, each of the proposed algorithms relies on the successful evaluation of zeroth and higher order (endpoint) derivatives of either of the ordinary basis functions (1) or of the non-negative normalized B-basis (4). The order of (endpoint) derivatives that have to be evaluated increases proportionally with the dimension $n+1$ of the underlying EC space. Due to floating point arithmetical operations, the maximal dimension for which one does not bump into numerical stability problems depends on the type of the ordinary basis functions of the given EC space – depending on the case, it may be smaller or greater, but considering that, in practice, curves and surfaces are mostly composed of smoothly joined lower order arcs and patches, a clever implementation of the proposed algorithms can be useful in case of real-life applications.

1.3 Structure

The rest of the manuscript is organized as follows. Section 2 consists of four subsections that detail and study *general* algorithms that can be used 1) to construct and differentiate the bases (1) and (4) in EC spaces that comprise the constants and can be identified with the solution spaces of differential equations of type (9); 2) to elevate the dimensions of the underlying EC spaces and consequently the order of the induced EC B-curves and B-surfaces; 3) to subdivide EC B-curves and B-surfaces; 4) to generate basis transformation matrices for the control point based exact description (i.e., B-representation) of ordinary integral curves and surfaces given in traditional parametric form. Using class diagrams and brief descriptions, Section 3 presents the main data structures and methods of our implementation. Section 4 provides further examples, run-time statistics and gives advices for handling possible numerical instabilities. Section 5 closes the manuscript with our summary and conclusions.

2 Theoretical results and proposed algorithms

In order to formulate the input and output of our algorithms, we define the following control point based integral curves and surfaces.

Definition 2.1 (EC B-curves). *The convex combination*

$$\mathbf{c}_n(u) = \sum_{i=0}^n \mathbf{p}_i b_{n,i}(u), \quad u \in [\alpha, \beta], \quad \mathbf{p}_i = \left[p_i^\ell \right]_{\ell=0}^{\delta-1} \in \mathbb{R}^\delta, \quad \delta \geq 2 \quad (11)$$

described by means of the non-negative normalized B-basis (4) is called an EC B-curve of order n , where $[\mathbf{p}_i]_{i=0}^n$ denotes its control polygon.

Definition 2.2 (EC B-surfaces). *Denoting by*

$$\mathcal{B}_{n_r}^{\alpha_r, \beta_r} = \{ b_{n_r, i_r}(u_r; \alpha_r, \beta_r) : u_r \in [\alpha_r, \beta_r] \}_{i_r=0}^{n_r}, \quad r = 0, 1$$

two non-negative normalized B-basis of some EC spaces and using the tensor product of curves of type (11), one can define the EC B-surface

$$\mathbf{s}_{n_0, n_1}(u_0, u_1) = \sum_{i_0=0}^{n_0} \sum_{i_1=0}^{n_1} \mathbf{p}_{i_0, i_1} b_{n_0, i_0}(u_0; \alpha_0, \beta_0) b_{n_1, i_1}(u_1; \alpha_1, \beta_1), \quad \mathbf{p}_{i_0, i_1} = \left[p_{i_0, i_1}^\ell \right]_{\ell=0}^2 \in \mathbb{R}^3 \quad (12)$$

of order (n_0, n_1) , where the matrix $[\mathbf{p}_{i_0, i_1}]_{i_0=0, i_1=0}^{n_0, n_1}$ forms a control net.

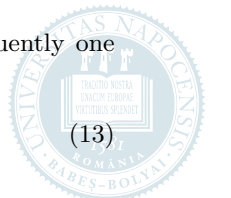
2.1 Construction and differentiation of non-negative normalized B-basis functions in a large class of EC spaces

As already stated in Section 1, our implementation assumes that the underlying EC space $\mathbb{S}_n^{\alpha, \beta}$ corresponds to the solution space of a constant-coefficient homogeneous linear differential equation of type (9). This is not necessary for the correctness of the algorithms that will be presented in the forthcoming sections. The only reason for this additional assumption is the fact that in this case we have the possibility to handle a large family of (mixed) EC spaces in a unified way.

For example, if $\mathbf{i} = \sqrt{-1}$, $a, b \in \mathbb{R}$ and $z = a + \mathbf{i}b$ is an m th order ($m \geq 1$) zero of the characteristic polynomial (10), then based on its real and imaginary parts one has that:

- if $a, b \in \mathbb{R} \setminus \{0\}$, the conjugate complex number \bar{z} is also a root of multiplicity m and consequently one obtains an algebraic-exponential-trigonometric (AET) mixed EC subspace

$$\left\langle \left\{ u^r e^{au} \cos(bu), u^r e^{au} \sin(bu) : u \in [\alpha, \beta] \right\}_{r=0}^{m-1} \right\rangle \subseteq \mathbb{S}_n^{\alpha, \beta}; \quad (13)$$



– if $a \neq 0$, but $b = 0$, then one has the algebraic-exponential (AE) mixed EC subspace

$$\left\langle \left\{ u^r e^{au} : u \in [\alpha, \beta] \right\}_{r=0}^{m-1} \right\rangle \subseteq \mathbb{S}_n^{\alpha, \beta}; \quad (14)$$

– if $a = 0$, but $b \neq 0$, then one obtains the algebraic-trigonometric (AT) mixed EC subspace

$$\left\langle \left\{ u^r \cos(bu), u^r \sin(bu) : u \in [\alpha, \beta] \right\}_{r=0}^{m-1} \right\rangle \subseteq \mathbb{S}_n^{\alpha, \beta}; \quad (15)$$

– if $a = b = 0$ then one has the polynomial (P) EC subspace

$$\left\langle \left\{ u^r : u \in [\alpha, \beta] \right\}_{r=0}^{m-1} \right\rangle \subseteq \mathbb{S}_n^{\alpha, \beta}. \quad (16)$$

This means that one can easily define ordinary (mixed) basis functions by simply specifying the factorization of the characteristic polynomial (10), i.e., one can create (mixed) EC spaces at run-time in an interactive way. As we will see, the zeroth and higher order (endpoint) derivatives of the ordinary basis function will play an important role in case of all proposed algorithms. In case of the aforementioned (mixed) EC subspaces one can overload function operators to compute the required derivatives for arbitrarily fixed orders – this possibility also motivates our assumption on the structure of the underlying EC space. Moreover, in real-world engineering, computer-aided design and manufacturing applications, usually one defines traditional parametric curves and surfaces by means of the ordinary basis functions presented above and, in our opinion, it would be nice to have a unified framework in which – apart from general order elevation and subdivision – one is also able to describe exactly important curves and surfaces by using control points and non-negative normalized B-basis functions.

In order to have normalizable bases in the vector space $\mathbb{S}_n^{\alpha, \beta}$, we also have to assume that $z = 0$ is at least a first order zero of the characteristic polynomial (10).

Once we have created an EC space of type $\mathbb{S}_n^{\alpha, \beta}$ by defining its ordinary basis $\mathcal{F}_n^{\alpha, \beta}$, we also have to generate its unique non-negative normalized B-basis $\mathcal{B}_n^{\alpha, \beta}$. In order to achieve this and to be as self-contained as possible, we recall the construction process [1] of $\mathcal{B}_n^{\alpha, \beta}$. As we will see, the steps of this process can be fully implemented in case of the aforementioned (mixed) EC spaces.

Denote by

$$W_{[v_{n,0}, v_{n,1}, \dots, v_{n,n}]}(u) := \left[v_{n,i}^{(j)}(u) \right]_{i=0, j=0}^{n, n} \quad (17)$$

the Wronskian matrix of those particular integrals

$$v_{n,i} := \sum_{k=0}^n \rho_{i,k} \varphi_{n,k} \in \mathbb{S}_n^{\alpha, \beta}, \quad i = 0, 1, \dots, n \quad (18)$$

of (9) that correspond to the initial conditions

$$\begin{cases} v_{n,i}^{(j)}(\alpha) = 0, & j = 0, \dots, i-1, \\ v_{n,i}^{(i)}(\alpha) = 1, \\ v_{n,i}^{(j)}(\beta) = 0, & j = 0, \dots, n-1-i, \end{cases} \quad (19)$$

i.e., the system $\{v_{n,i}(u) : u \in [\alpha, \beta]\}_{i=0}^n$ is a bicanonical basis on the interval $[\alpha, \beta]$ such that the Wronskian (17) at $u = \alpha$ is a lower triangular matrix with positive (unit) diagonal entries.

Consider the functions (or Wronskian determinants)

$$w_{n,i}(u) := \det W_{[v_{n,i}, v_{n,i+1}, \dots, v_{n,n}]}(u), \quad i = \left\lfloor \frac{n}{2} \right\rfloor, \left\lfloor \frac{n}{2} \right\rfloor + 1, \dots, n, \quad (20)$$

define the critical length

$$\ell_n^* := \min_{i=\left\lfloor \frac{n}{2} \right\rfloor, \left\lfloor \frac{n}{2} \right\rfloor + 1, \dots, n} \min \{ |u - \alpha| : w_{n,i}(u) = 0, u \neq \alpha \} \quad (21)$$

and, in what follows, assume that $\beta \in (\alpha, \alpha + \ell_n^*)$ is an arbitrarily fixed shape parameter (we write $\ell_n^* = +\infty$ whenever the Wronskian determinants (20) do not have real zeros other than α).

Consider the Wronskian matrix $W_{[v_{n,n}, v_{n,n-1}, \dots, v_{n,0}]}(\beta)$ of the reverse ordered system $\{v_{n,n-i}(u) : u \in [\alpha, \beta]\}_{i=0}^n$ at the parameter value $u = \beta$ and obtain its Doolittle-type LU factorization

$$L \cdot U = W_{[v_{n,n}, v_{n,n-1}, \dots, v_{n,0}]}(\beta),$$

where L is a lower triangular matrix with unit diagonal, while U is a non-singular upper triangular matrix. Calculate the inverse matrices

$$U^{-1} := \begin{bmatrix} \mu_{0,0} & \mu_{0,1} & \cdots & \mu_{0,n} \\ 0 & \mu_{1,1} & \cdots & \mu_{1,n} \\ \vdots & \vdots & \ddots & \vdots \\ 0 & 0 & \cdots & \mu_{n,n} \end{bmatrix}, \quad L^{-1} := \begin{bmatrix} \lambda_{0,0} & 0 & \cdots & 0 \\ \lambda_{1,0} & \lambda_{1,1} & \cdots & 0 \\ \vdots & \vdots & \ddots & \vdots \\ \lambda_{n,0} & \lambda_{n,1} & \cdots & \lambda_{n,n} \end{bmatrix}$$



and construct the non-negative normalized B-basis

$$\mathcal{B}_n^{\alpha,\beta} = \left\{ b_{n,i}(u) = \lambda_{n-i,0} \tilde{b}_{n,i}(u) : u \in [\alpha, \beta] \right\}_{i=0}^n \quad (22)$$

defined by

$$[\tilde{b}_{n,n}(u) \tilde{b}_{n,n-1}(u) \cdots \tilde{b}_0(u)] := [v_{n,n}(u) v_{n,n-1}(u) \cdots v_{n,0}(u)] \cdot U^{-1}$$

and

$$[\lambda_{0,0} \lambda_{1,0} \cdots \lambda_{n,0}]^T := L^{-1} \cdot [1 \ 0 \ \cdots \ 0]^T.$$

If the characteristic polynomial (10) is an either even or odd function, then the underlying EC space $\mathbb{S}_n^{\alpha,\beta}$ is invariant under reflections, and in this special case one obtains the symmetry

$$b_{n,i}(u) = b_{n,n-i}(\alpha + \beta - u), \quad \forall u \in [\alpha, \beta], \quad i = 0, 1, \dots, \left\lfloor \frac{n}{2} \right\rfloor,$$

i.e., we only need to determine the half of the basis functions (22).

Summarizing the calculations of the current section, we can state the next theorem that will be very important both in the formulation and in the implementation of all proposed algorithms.

Theorem 2.1 (Differentiation of B-basis functions). *In general, the zeroth and higher order differentiation of the constructed non-negative normalized B-basis functions (22) can be reduced to the evaluation of formulas*

$$\begin{aligned} b_{n,n-i}^{(j)}(u) &= \lambda_{i,0} \tilde{b}_{n,n-i}^{(j)}(u) \\ &= \lambda_{i,0} \sum_{r=0}^i \mu_{r,i} v_{n,n-r}^{(j)}(u) \\ &= \lambda_{i,0} \sum_{r=0}^i \mu_{r,i} \sum_{k=0}^n \rho_{n-r,k} \varphi_{n,k}^{(j)}(u), \quad \forall u \in [\alpha, \beta], \quad i = 0, 1, \dots, n. \end{aligned} \quad (23)$$

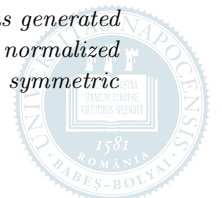
Naturally, if the underlying EC space is reflection invariant, then formulas (23) have to be applied only for indices $i = 0, 1, \dots, \left\lfloor \frac{n}{2} \right\rfloor$, since in this special case one also has that

$$b_{n,i}^{(j)}(u) = (-1)^j b_{n,n-i}^{(j)}(\alpha + \beta - u), \quad \forall u \in [\alpha, \beta], \quad i = 0, 1, \dots, \left\lfloor \frac{n}{2} \right\rfloor. \quad (24)$$

Figs. 1 and 2 provide short examples in algebraic-trigonometric and exponential EC spaces, respectively. Both figures were generated by the help of the proposed function library. (After evaluation and rendering, only the L^AT_EX-like labels of the obtained basis functions and some other descriptive elements were added in a post-processing phase. Here we have only illustrated the zeroth order derivatives of the automatically generated ordinary and non-negative normalized B-basis functions.)

Example 2.1 (A reflection invariant algebraic-trigonometric EC space). *Consider the differential equation $v^{(9)}(u) + 6v^{(7)}(u) + 9v^{(5)}(u) + 4v^{(3)}(u) = 0$, $u \in [-\frac{\pi}{2}, \frac{\pi}{2}]$ and observe that its characteristic polynomial is an odd function that admits the factorization $p_9(z) = z^3 \prod_{k=1}^2 (z^2 + k^2)^{3-k}$, $z \in \mathbb{C}$, i.e., the 9-dimensional algebraic-trigonometric solution space $\mathbb{A}\mathbb{T}_8^{-\frac{\pi}{2}, \frac{\pi}{2}}$ of the equation is reflection invariant and is spanned by the ordinary basis $\mathcal{F}_8^{-\frac{\pi}{2}, \frac{\pi}{2}} = \{\varphi_{8,0}(u) \equiv 1, \varphi_{8,1}(u) = u, \varphi_{8,2}(u) = u^2, \varphi_{8,3}(u) = \cos(u), \varphi_{8,4}(u) = \sin(u), \varphi_{8,5}(u) = u \cos(u), \varphi_{8,6}(u) = u \sin(u), \varphi_{8,7}(u) = \cos(2u), \varphi_{8,8}(u) = \sin(2u) : u \in [-\frac{\pi}{2}, \frac{\pi}{2}]\}$. Providing the (higher order) zeros of p_9 as input parameters, our function library is able to differentiate and render both the ordinary basis and the non-negative normalized B-basis of $\mathbb{A}\mathbb{T}_8^{-\frac{\pi}{2}, \frac{\pi}{2}}$. The output of our implementation can be seen in Fig. 1.*

Example 2.2 (A not reflection invariant exponential EC space). *Consider the differential equation $v^{(5)}(u) - \frac{5}{2}v^{(4)}(u) + \frac{35}{16}v^{(3)}(u) - \frac{25}{32}v^{(2)}(u) + \frac{3}{32}v^{(1)}(u) = 0$, $u \in [-2, \frac{1}{2}]$ and observe that its characteristic polynomial can be factorized into the form $p_5(z) = \prod_{i=0}^4 (z - \omega_i)$, where $\{\omega_i = \frac{i}{4}\}_{i=0}^4$, i.e., the solution space of the equation is the 5-dimensional exponential EC space $\mathbb{S}_4^{-2, \frac{1}{2}} = \langle \mathcal{F}_4^{-2, \frac{1}{2}} \rangle = \langle \{\varphi_{4,i}(u) = e^{\omega_i u} : u \in [-2, \frac{1}{2}]\}_{i=0}^4 \rangle$. Fig. 2 was generated by means of the proposed function library and illustrates both the ordinary basis and the non-negative normalized B-basis of the space. Compared with Example 2.1, it can be observed that the B-basis functions are not symmetric under the reflection of the definition domain.*



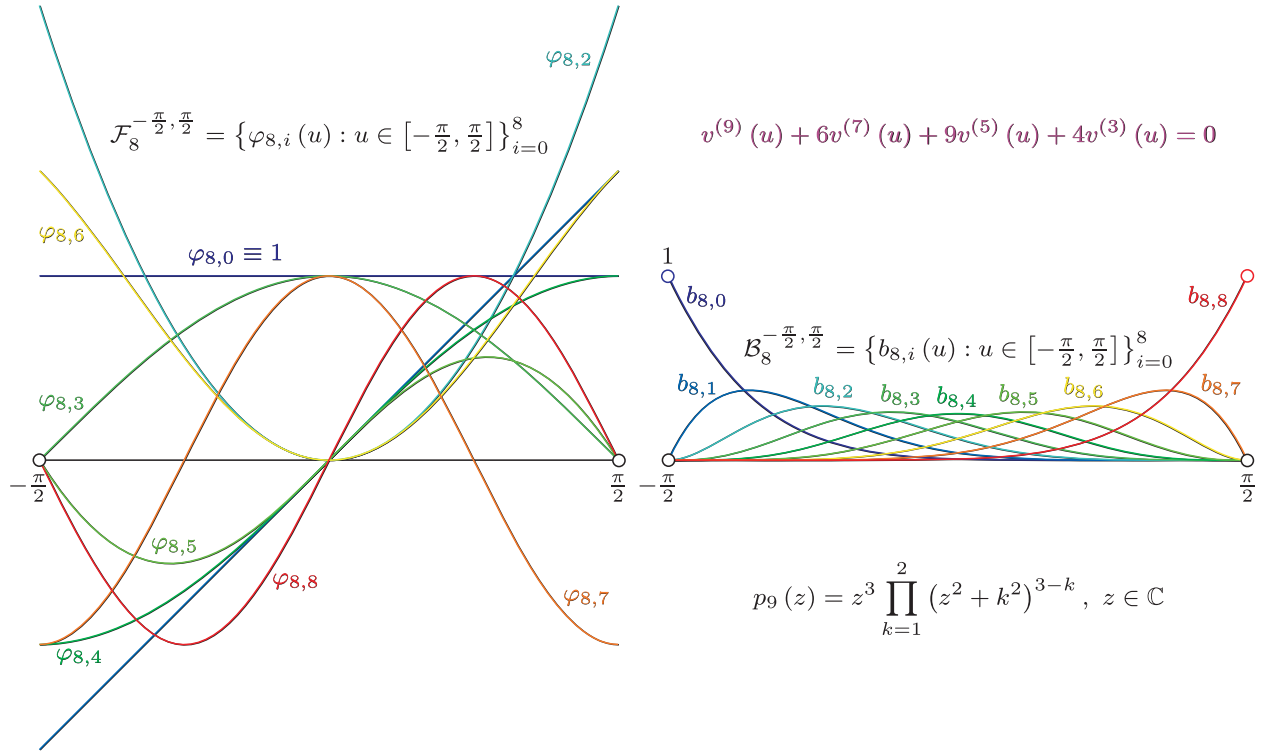


Fig. 1: The figure illustrates both the ordinary basis and the non-negative normalized B-basis of the 9-dimensional reflection invariant algebraic-trigonometric EC space $\mathbb{A}\mathbb{T}_8^{-\frac{\pi}{2}, \frac{\pi}{2}}$ described in Example 2.1.

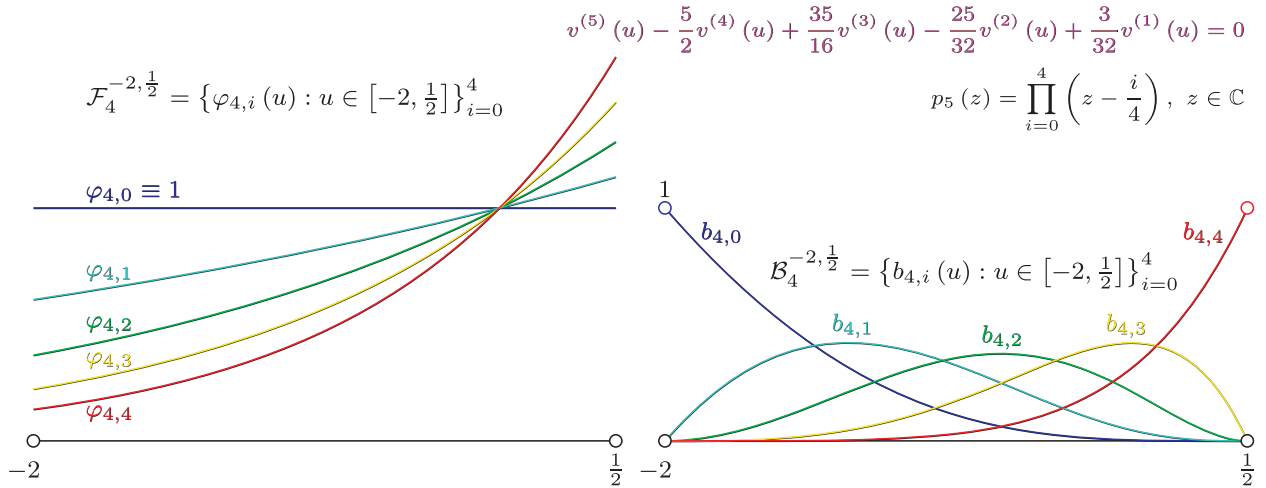


Fig. 2: The figure illustrates both the ordinary basis and the non-negative normalized B-basis of the 5-dimensional not reflection invariant exponential EC space $\mathbb{S}_4^{-2, \frac{1}{2}}$ described in Example 2.2.

2.2 General dimension and order elevation

Consider the EC spaces $\mathbb{S}_n^{\alpha, \beta}$ and $\mathbb{S}_{n+1}^{\alpha, \beta}$ such that $1 \in \mathbb{S}_n^{\alpha, \beta} \subset \mathbb{S}_{n+1}^{\alpha, \beta}$ and assume that their unique non-negative normalized B-bases are $\{b_{n,i}(u) : u \in [\alpha, \beta]\}_{i=0}^n$ and $\{b_{n+1,i}(u) : u \in [\alpha, \beta]\}_{i=0}^{n+1}$, respectively.

Since, in this case, both bases fulfill the corresponding order variant of the endpoint conditions (6)–(8), it follows that the relation between the smaller and higher order basis functions can be described as the linear combination

$$b_{n,i}(u) = \xi_{n,i} b_{n+1,i}(u) + \zeta_{n,i+1} b_{n+1,i+1}(u), \quad \forall u \in [\alpha, \beta], \quad \forall i = 0, 1, \dots, n, \quad (25)$$

where the real numbers $\{\xi_{n,i}, \zeta_{n,i+1}\}_{i=0}^n$ are unknown at the moment. (If one would introduce other higher order basis functions into the linear combination (25), then we would obtain non-zero endpoint derivatives contradicting conditions (7) and (8).) The non-negativity of the unknown scalars $\{\xi_{n,i}, \zeta_{n,i+1}\}_{i=0}^n$ is also a consequence of the conditions (6)–(8).

Using that both bases are normalized, observe that by identifying the coefficients of the higher order basis functions that appear in the identity

$$\begin{aligned} 1 &\equiv \sum_{i=0}^n b_{n,i}(u) \stackrel{(25)}{=} \sum_{i=0}^n (\xi_{n,i} b_{n+1,i}(u) + \zeta_{n,i+1} b_{n+1,i+1}(u)) \\ &= \sum_{i=0}^n \xi_{n,i} b_{n+1,i}(u) + \sum_{i=0}^n \zeta_{n,i+1} b_{n+1,i+1}(u) \end{aligned}$$



$$\begin{aligned}
&= \sum_{i=0}^n \xi_{n,i} b_{n+1,i}(u) + \sum_{i=1}^{n+1} \zeta_{n,i} b_{n+1,i}(u) \\
&= \xi_{n,0} b_{n+1,0}(u) + \sum_{i=1}^n (\xi_{n,i} + \zeta_{n,i}) b_{n+1,i}(u) + \zeta_{n,n+1} b_{n+1,n+1}(u) \\
&= \sum_{i=0}^{n+1} 1 \cdot b_{n+1,i}(u), \quad \forall u \in [\alpha, \beta],
\end{aligned}$$

one obtains the additional relations

$$\xi_{n,0} = \zeta_{n,n+1} = 1, \quad (26)$$

$$\xi_{n,i} + \zeta_{n,i} = 1, \quad i = 1, \dots, n. \quad (27)$$

Therefore the linear combination (25) becomes a convex one, and differentiating it for each order $i = 1, \dots, n$ at the parameter value $u = \alpha$, based on the n th and $(n+1)$ th order variants of condition (7), one obtains the expressions

$$0 < b_{n,i}^{(i)}(\alpha) = \xi_{n,i} b_{n+1,i}^{(i)}(\alpha) + \zeta_{n,i+1} b_{n+1,i+1}^{(i)}(\alpha) = \xi_{n,i} b_{n+1,i}^{(i)}(\alpha), \quad b_{n+1,i}^{(i)}(\alpha) > 0, \quad i = 1, \dots, n$$

that combined with relations (27) finally lead to the values

$$\xi_{n,i} = \frac{b_{n,i}^{(i)}(\alpha)}{b_{n+1,i}^{(i)}(\alpha)} \in (0, 1), \quad \zeta_{n,i} = 1 - \xi_{n,i} = 1 - \frac{b_{n,i}^{(i)}(\alpha)}{b_{n+1,i}^{(i)}(\alpha)} \in (0, 1), \quad i = 1, \dots, n.$$

Observe that the unique scalars $\{\xi_{n,i}, \zeta_{n,i} = 1 - \xi_{n,i}\}_{i=1}^n$ can also be determined by means of first and higher order endpoint derivatives that correspond to the parameter value $u = \beta$. Indeed, by performing the index transformation $i \rightarrow n - i$ in relations (25) and by differentiating the obtained expressions in order $i = 1, \dots, n$ at $u = \beta$, and, finally, by considering the n th and $(n+1)$ th order variant of the endpoint conditions (8), one obtains that

$$\begin{aligned}
0 \neq b_{n,n-i}^{(i)}(\beta) &= \xi_{n,n-i} b_{n+1,n-i}^{(i)}(\beta) + \zeta_{n,n+1-i} b_{n+1,n+1-i}^{(i)}(\beta) \\
&= \zeta_{n,n+1-i} b_{n+1,n+1-i}^{(i)}(\beta), \quad b_{n+1,n+1-i}^{(i)}(\beta) \neq 0, \quad i = 1, \dots, n,
\end{aligned}$$

which combined with identities (27) lead to the values

$$\begin{aligned}
\zeta_{n,n+1-i} &= \frac{b_{n,n-i}^{(i)}(\beta)}{b_{n+1,n+1-i}^{(i)}(\beta)} \in (0, 1), \quad i = 1, \dots, n, \\
\xi_{n,n+1-i} &= 1 - \zeta_{n,n+1-i} = 1 - \frac{b_{n,n-i}^{(i)}(\beta)}{b_{n+1,n+1-i}^{(i)}(\beta)} \in (0, 1), \quad i = 1, \dots, n,
\end{aligned}$$

where we have also used the fact that the derivatives appearing in the nominator and denominator of each fraction have the same sign.

Summarizing the calculations of the section and ensuring greater efficiency and numerical stability for our implementation of the just presented general order (dimension) elevation method, we formulate the next theorem.

Theorem 2.2 (General order elevation). *Using the notations of the section, the n th order EC B-curve (11) fulfills the identity*

$$\mathbf{c}_n(u) = \sum_{i=0}^n \mathbf{p}_i b_{n,i}(u) \equiv \sum_{i=0}^{n+1} \mathbf{p}_{1,i} b_{n+1,i}(u) =: \mathbf{c}_{n+1}(u), \quad \forall u \in [\alpha, \beta],$$

where $\mathbf{p}_{1,0} = \mathbf{p}_0$, $\mathbf{p}_{1,n+1} = \mathbf{p}_n$ and

$$\begin{aligned}
\mathbf{p}_{1,i} &= \zeta_{n,i} \mathbf{p}_{i-1} + \xi_{n,i} \mathbf{p}_i \\
&= \left(1 - \frac{b_{n,i}^{(i)}(\alpha)}{b_{n+1,i}^{(i)}(\alpha)} \right) \mathbf{p}_{i-1} + \frac{b_{n,i}^{(i)}(\alpha)}{b_{n+1,i}^{(i)}(\alpha)} \mathbf{p}_i, \quad i = 1, \dots, \left\lfloor \frac{n}{2} \right\rfloor,
\end{aligned} \quad (28)$$

$$\begin{aligned}
\mathbf{p}_{1,n+1-i} &= \zeta_{n,n+1-i} \mathbf{p}_{n-i} + \xi_{n,n+1-i} \mathbf{p}_{n+1-i} \\
&= \frac{b_{n,n-i}^{(i)}(\beta)}{b_{n+1,n+1-i}^{(i)}(\beta)} \mathbf{p}_{n-i} + \left(1 - \frac{b_{n,n-i}^{(i)}(\beta)}{b_{n+1,n+1-i}^{(i)}(\beta)} \right) \mathbf{p}_{n+1-i}, \quad i = 1, \dots, \left\lfloor \frac{n+1}{2} \right\rfloor.
\end{aligned} \quad (29)$$

Although Theorem 2.2 is valid for any nested EC spaces that fulfill the conditions $1 \in \mathbb{S}_n^{\alpha,\beta} \subset \mathbb{S}_{n+1}^{\alpha,\beta}$, in case of our implementation, we always assume that the higher dimensional EC space $\mathbb{S}_{n+1}^{\alpha,\beta}$ can also be identified with the solution space of a constant-coefficient homogeneous linear differential equation. Naturally, the results of Theorem 2.2 can also be extended to the general order elevation of EC B-surfaces of type (12) and our function library ensures this possibility as well as it is illustrated in Fig. 3 associated with the next example.

Example 2.3 (Order elevation of B-surfaces). Consider the ordinary exponential-trigonometric integral surface

$$\mathbf{s}(u_0, u_1) = \begin{bmatrix} s^0(u_0, u_1) \\ s^1(u_0, u_1) \\ s^2(u_0, u_1) \end{bmatrix} = \begin{bmatrix} (1 - e^{\omega_0 u_0}) \cos(u_0) \left(\frac{5}{4} + \cos(u_1)\right) \\ (e^{\omega_0 u_0} - 1) \sin(u_0) \left(\frac{5}{4} + \cos(u_1)\right) \\ 7 - e^{\omega_1 u_0} - \sin(u_1) + e^{\omega_0 u_0} \sin(u_1) \end{bmatrix}, \quad (30)$$

where $(u_0, u_1) \in \left[\frac{7\pi}{2}, \frac{49\pi}{8}\right] \times \left[-\frac{\pi}{3}, \frac{5\pi}{3}\right]$, $\omega_0 = \frac{1}{6\pi}$ and $\omega_1 = \frac{1}{3\pi}$. In order to describe any restriction (i.e., patch) $\mathbf{s}|_{[\alpha_0, \beta_0] \times [\alpha_1, \beta_1]}$ by means of EC B-surfaces of type (12), in directions u_0 and u_1 one needs to define EC spaces that include the subspaces $\mathbb{E}\mathbb{T}_6^{\alpha_0, \beta_0} := \langle \mathcal{E}\mathcal{T}_6^{\alpha_0, \beta_0} \rangle := \langle \{1, \cos(u_0), \sin(u_0), e^{\omega_0 u_0}, e^{\omega_1 u_0}, e^{\omega_0 u_0} \cos(u_0), e^{\omega_0 u_0} \sin(u_0) : u_0 \in [\alpha_0, \beta_0]\} \rangle$ and $\mathbb{T}_2^{\alpha_1, \beta_1} := \langle \mathcal{T}_2^{\alpha_1, \beta_1} \rangle := \langle \{1, \cos(u_1), \sin(u_1) : u_1 \in [\alpha_1, \beta_1]\} \rangle$, respectively, where the interval lengths $\beta_0 - \alpha_0 > 0$ and $\beta_1 - \alpha_1 > 0$ must be less than the critical lengths of the corresponding EC spaces. Observe that $\mathbb{E}\mathbb{T}_6^{\alpha_0, \beta_0}$ and $\mathbb{T}_2^{\alpha_1, \beta_1}$ can be identified with the solution spaces of those differential equations of type (9) whose characteristic polynomials can be factorized into $p_7(z) = z(z - \mathbf{i})(z + \mathbf{i})(z - \omega_0)(z - \omega_1)(z - (\omega_0 - \mathbf{i}))(z - (\omega_0 + \mathbf{i}))$ and $p_3(z) = z(z - \mathbf{i})(z + \mathbf{i})$, respectively, where $z \in \mathbb{C}$. Providing the zeros of these polynomials as input parameters, the proposed function library is able to perform general order elevation either by increasing the order of one of these zeros, or by specifying new ones of single or higher multiplicity. Case (a) of Fig. 3 illustrates a control net of minimal size that allows the control point based exact description of the surface patch $\mathbf{s}|_{\left[\frac{11\pi}{2}, \frac{49\pi}{8}\right] \times \left[-\frac{\pi}{3}, \frac{\pi}{3}\right]}$, possible order elevations of which can be done in infinitely many ways, e.g. in case (b) of Fig. 3 in directions u_0 and u_1 we have applied the non-negative B-bases of the higher dimensional algebraic-exponential-trigonometric and algebraic-trigonometric EC spaces $\mathbb{A}\mathbb{E}\mathbb{T}_7^{\alpha_0, \beta_0} := \langle \mathcal{E}\mathcal{T}_6^{\alpha_0, \beta_0} \cup \{u_0 : u_0 \in [\alpha_0, \beta_0]\} \rangle$ and $\mathbb{A}\mathbb{T}_3^{\alpha_1, \beta_1} := \langle \mathcal{T}_2^{\alpha_1, \beta_1} \cup \{u_1 : u_1 \in [\alpha_1, \beta_1]\} \rangle$, respectively, while in case (c) of Fig. 3 we have considered the exponential-trigonometric and algebraic-trigonometric EC spaces $\mathbb{E}\mathbb{T}_8^{\alpha_0, \beta_0} := \langle \mathcal{E}\mathcal{T}_6^{\alpha_0, \beta_0} \cup \{e^{-\omega_0 u_0}, e^{-\omega_1 u_0} : u_0 \in [\alpha_0, \beta_0]\} \rangle$ and $\mathbb{A}\mathbb{T}_4^{\alpha_1, \beta_1} := \langle \mathcal{T}_2^{\alpha_1, \beta_1} \cup \{u_1 \cos(u_1), u_1 \sin(u_1) : u_1 \in [\alpha_1, \beta_1]\} \rangle$, respectively. Observe that in case (b) we have increased in both directions the order of the already existing zero $z = 0$, i.e., we defined the new characteristic polynomials $p_8(z) = zp_7(z)$ and $p_4(z) = zp_3(z)$, while in case (c) we applied the polynomials $p_9(z) = (z + \omega_0)(z + \omega_1)p_7(z)$ and $p_5(z) = (z - \mathbf{i})(z + \mathbf{i})p_3(z)$, i.e., in directions u_0 and u_1 we have introduced the new zeros $z = -\omega_0$ and $z = -\omega_1$ and increased the multiplicity of the existing zeros $z = \pm \mathbf{i}$ from 1 to 2, respectively.

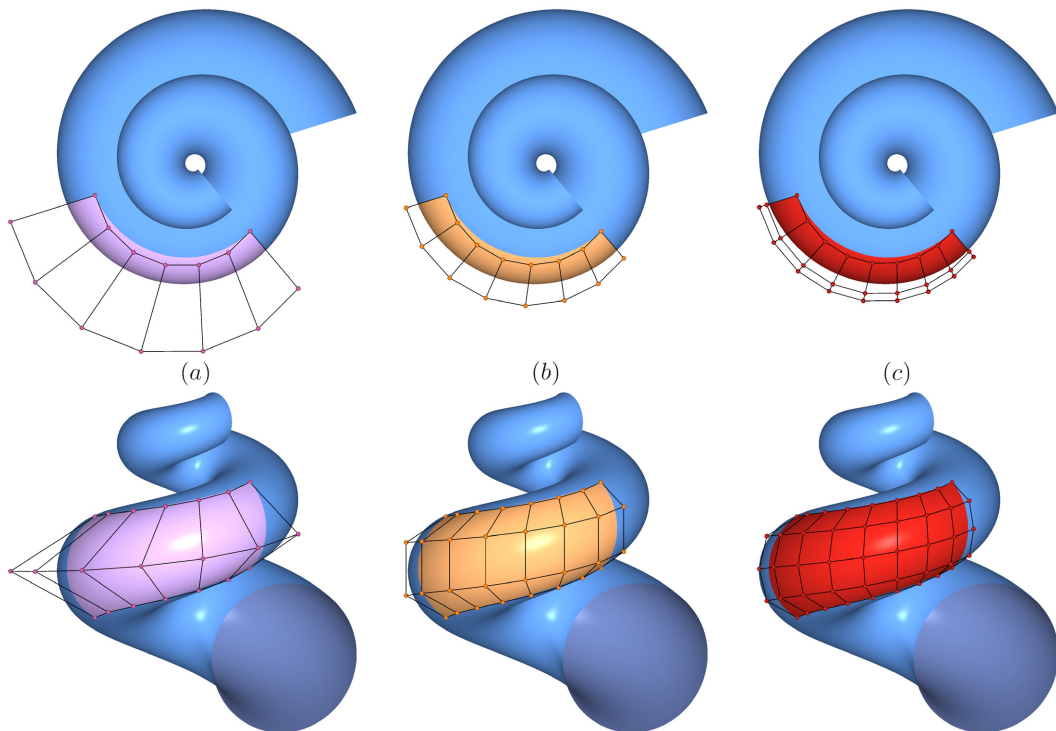


Fig. 3: (a) Control point based exact description of the patch $\mathbf{s}|_{\left[\frac{11\pi}{2}, \frac{49\pi}{8}\right] \times \left[-\frac{\pi}{3}, \frac{\pi}{3}\right]}$ of the ordinary exponential-trigonometric integral surface (30) by means of an EC B-surface of minimal order. Cases (b) and (c) illustrate two possible order elevations of the same patch by using the non-negative B-bases of higher dimensional EC spaces. (More details can be found in Example 2.3. All images were rendered by means of the proposed function library.)

2.3 General B-algorithm

Theoretically, every non-negative normalized B-basis implies a B-algorithm for the subdivision of EC B-curves like (11), i.e., for an arbitrarily fixed parameter value $\gamma \in (\alpha, \beta)$ there exists a recursive corner cutting de



Casteljau-like algorithm that starts with the initial conditions $\mathbf{p}_i^0(\gamma) \equiv \mathbf{p}_i$, $i = 0, 1, \dots, n$ and recursively defines the subdivision points

$$\mathbf{p}_i^j(\gamma) = \left(1 - \xi_i^j(\gamma)\right) \cdot \mathbf{p}_i^{j-1}(\gamma) + \xi_i^j(\gamma) \cdot \mathbf{p}_{i+1}^{j-1}(\gamma), \quad i = 0, \dots, n-j, \quad j = 1, \dots, n, \quad (31)$$

where the explicit closed form of the blending functions $\left\{\xi_i^j : [\alpha, \beta] \rightarrow [0, 1]\right\}_{i=0, j=1}^{n-j, n}$, in general, are either not known, or, apart from some very special cases (like Bézier curves), usually have non-linear complicated expressions even in low-dimensional EC spaces.

Let $\mathcal{B}_n^{\alpha, \gamma} := \{b_{n,i}(u; \alpha, \gamma) : u \in [\alpha, \gamma]\}_{i=0}^n$ and $\mathcal{B}_n^{\gamma, \beta} := \{b_{n,i}(u; \gamma, \beta) : u \in [\gamma, \beta]\}_{i=0}^n$ be the unique non-negative normalized B-bases of the restricted EC spaces $\mathbb{S}_n^{\alpha, \gamma} := \text{span } \mathcal{F}_n^{\alpha, \gamma} := \text{span } \mathcal{F}_n^{\alpha, \beta} \Big|_{[\alpha, \gamma]}$ and $\mathbb{S}_n^{\gamma, \beta} := \text{span } \mathcal{F}_n^{\gamma, \beta} := \text{span } \mathcal{F}_n^{\alpha, \beta} \Big|_{[\gamma, \beta]}$, respectively, and consider the diagonal entries $\{\boldsymbol{\lambda}_i(\gamma) := \mathbf{p}_0^i(\gamma)\}_{i=0}^n$ and $\{\boldsymbol{\varrho}_i(\gamma) := \mathbf{p}_i^{n-i}(\gamma)\}_{i=0}^n$ of the triangular scheme

$$\begin{array}{lll} \mathbf{p}_0 & =: & \boldsymbol{\lambda}_0(\gamma) \\ \mathbf{p}_1 & & \mathbf{p}_0^1(\gamma) =: \boldsymbol{\lambda}_1(\gamma) \\ \mathbf{p}_2 & & \mathbf{p}_1^1(\gamma) \quad \mathbf{p}_0^2(\gamma) =: \boldsymbol{\lambda}_2(\gamma) \\ \vdots & & \vdots \quad \dots \quad \mathbf{p}_0^n(\gamma) =: \boldsymbol{\lambda}_n(\gamma) =: \boldsymbol{\varrho}_0(\gamma) \\ \mathbf{p}_{n-2} & & \mathbf{p}_{n-2}^1(\gamma) \quad \mathbf{p}_{n-2}^2(\gamma) =: \boldsymbol{\varrho}_{n-2}(\gamma) \\ \mathbf{p}_{n-1} & & \mathbf{p}_{n-1}^1(\gamma) =: \boldsymbol{\varrho}_{n-1}(\gamma) \\ \mathbf{p}_n & =: & \boldsymbol{\varrho}_n(\gamma) \end{array}$$

that can be associated with the recursive process (31). Linearly combining these points with the functions of the B-bases $\mathcal{B}_n^{\alpha, \gamma}$ and $\mathcal{B}_n^{\gamma, \beta}$, the EC B-curve (11) of order n can be subdivided into the left and right arcs

$$\boldsymbol{\ell}_n(u) := \sum_{i=0}^n \boldsymbol{\lambda}_i(\gamma) \cdot b_{n,i}(u; \alpha, \gamma) \equiv \mathbf{c}_n(u), \quad \forall u \in [\alpha, \gamma] \quad (32)$$

and

$$\boldsymbol{r}_n(u) := \sum_{i=0}^n \boldsymbol{\varrho}_i(\gamma) \cdot b_{n,i}(u; \gamma, \beta) \equiv \mathbf{c}_n(u), \quad \forall u \in [\gamma, \beta], \quad (33)$$

respectively, that also fulfill the identities

$$\boldsymbol{\ell}_n^{(j)}(u) = \mathbf{c}_n^{(j)}(u), \quad \forall u \in [\alpha, \gamma], \quad (34)$$

$$\boldsymbol{r}_n^{(j)}(u) = \mathbf{c}_n^{(j)}(u), \quad \forall u \in [\gamma, \beta] \quad (35)$$

for all differentiation orders $j \geq 0$.

We close the current section with a recursive method by means of which one can determine the unknown subdivision points $\{\boldsymbol{\lambda}_i(\gamma)\}_{i=0}^n$ and $\{\boldsymbol{\varrho}_i(\gamma)\}_{i=0}^n$ even in the absence of the usually unknown blending functions $\left\{\xi_i^j : [\alpha, \beta] \rightarrow [0, 1]\right\}_{i=0, j=1}^{n-j, n}$.

Theorem 2.3 (General B-algorithm). *Given an arbitrarily fixed parameter value $\gamma \in (\alpha, \beta)$ and starting with the initial conditions*

$$\boldsymbol{\lambda}_0(\gamma) = \mathbf{c}_n(\alpha) = \mathbf{p}_0, \quad (36)$$

$$\boldsymbol{\lambda}_n(\gamma) = \mathbf{c}_n(\gamma) = \boldsymbol{\varrho}_0(\gamma), \quad (37)$$

$$\boldsymbol{\varrho}_n(\gamma) = \mathbf{c}_n(\beta) = \mathbf{p}_n, \quad (38)$$

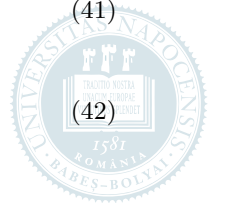
the unknown subdivision points $\{\boldsymbol{\lambda}_i(\gamma)\}_{i=0}^n$ and $\{\boldsymbol{\varrho}_i(\gamma)\}_{i=0}^n$ can be iteratively determined by means of the recursive formulas

$$\boldsymbol{\lambda}_i(\gamma) = \frac{1}{b_{n,i}^{(i)}(\alpha; \alpha, \gamma)} \left(\mathbf{c}_n^{(i)}(\alpha) - \sum_{j=0}^{i-1} \boldsymbol{\lambda}_j(\gamma) \cdot b_{n,j}^{(i)}(\alpha; \alpha, \gamma) \right), \quad i = 1, \dots, \left\lfloor \frac{n-1}{2} \right\rfloor, \quad (39)$$

$$\boldsymbol{\lambda}_{n-i}(\gamma) = \frac{1}{b_{n,n-i}^{(i)}(\gamma; \alpha, \gamma)} \left(\mathbf{c}_n^{(i)}(\gamma) - \sum_{j=0}^{i-1} \boldsymbol{\lambda}_{n-j}(\gamma) \cdot b_{n,n-j}^{(i)}(\gamma; \alpha, \gamma) \right), \quad i = 1, \dots, \left\lfloor \frac{n}{2} \right\rfloor, \quad (40)$$

$$\boldsymbol{\varrho}_i(\gamma) = \frac{1}{b_{n,i}^{(i)}(\gamma; \gamma, \beta)} \left(\mathbf{c}_n^{(i)}(\gamma) - \sum_{j=0}^{i-1} \boldsymbol{\varrho}_j(\gamma) \cdot b_{n,j}^{(i)}(\gamma; \gamma, \beta) \right), \quad i = 1, \dots, \left\lfloor \frac{n}{2} \right\rfloor, \quad (41)$$

$$\boldsymbol{\varrho}_{n-i}(\gamma) = \frac{1}{b_{n,n-i}^{(i)}(\beta; \gamma, \beta)} \left(\mathbf{c}_n^{(i)}(\beta) - \sum_{j=0}^{i-1} \boldsymbol{\varrho}_{n-j}(\gamma) \cdot b_{n,n-j}^{(i)}(\beta; \gamma, \beta) \right), \quad i = 1, \dots, \left\lfloor \frac{n-1}{2} \right\rfloor. \quad (42)$$



Proof. The calculation of the unknown subdivision points $\{\lambda_i(\gamma)\}_{i=0}^n$ and $\{\varrho_i(\gamma)\}_{i=0}^n$ can be reduced to the combined application of differentiation identities (34)–(35) and of those Hermite-type endpoint conditions (6)–(8) that are fulfilled by the non-negative normalized B-bases $\mathcal{B}_n^{\alpha,\beta}$, $\mathcal{B}_n^{\alpha,\gamma}$ and $\mathcal{B}_n^{\gamma,\beta}$ corresponding to the intervals $[\alpha, \beta]$, $[\alpha, \gamma]$ and $[\gamma, \beta]$, respectively.

For example, the initial condition (36) follows from the endpoint interpolation properties of the EC B-curves (11) and (32), since

$$\mathbf{c}_n(\alpha) = \sum_{i=0}^n \mathbf{p}_i \cdot b_{n,i}(\alpha; \alpha, \beta) = \mathbf{p}_0 = \lambda_0(\gamma) = \sum_{i=0}^n \lambda_i(\gamma) \cdot b_{n,i}(\alpha; \alpha, \gamma) = \ell_n(\alpha).$$

At the same time, for all differentiation orders $i = 1, \dots, \lfloor \frac{n-1}{2} \rfloor$ one obtains both the condition $b_{n,i}^{(i)}(\alpha; \alpha, \gamma) > 0$ and the equality

$$\begin{aligned} \mathbf{c}_n^{(i)}(\alpha) &= \ell_n^{(i)}(\alpha) \\ &= \sum_{j=0}^n \lambda_j(\gamma) \cdot b_{n,j}^{(i)}(\alpha; \alpha, \gamma) \\ &= \sum_{j=0}^i \lambda_j(\gamma) \cdot b_{n,j}^{(i)}(\alpha; \alpha, \gamma) \\ &= \sum_{j=0}^{i-1} \lambda_j(\gamma) \cdot b_{n,j}^{(i)}(\alpha; \alpha, \gamma) + \lambda_i(\gamma) \cdot b_{n,i}^{(i)}(\alpha; \alpha, \gamma), \end{aligned}$$

from which follows exactly formula (39) for the unknown subdivision point $\lambda_i(\gamma)$. The remaining recursive formulas (40)–(42) can be proved in a similar way. Observe that each recursion would also be valid for arbitrary values of the index $i \in \{1, \dots, n\}$. In the statement of the theorem we have restricted the index domain of each formula, since the maximum order of B-basis function derivatives that have to be evaluated has to be as small as possible in order to ensure greater efficiency and numerical stability for the just presented general B-algorithm. \square

The subdivision technique presented in Theorem 2.3 can also be extended to EC B-surfaces of the type (12) as it is shown in Fig. 4.

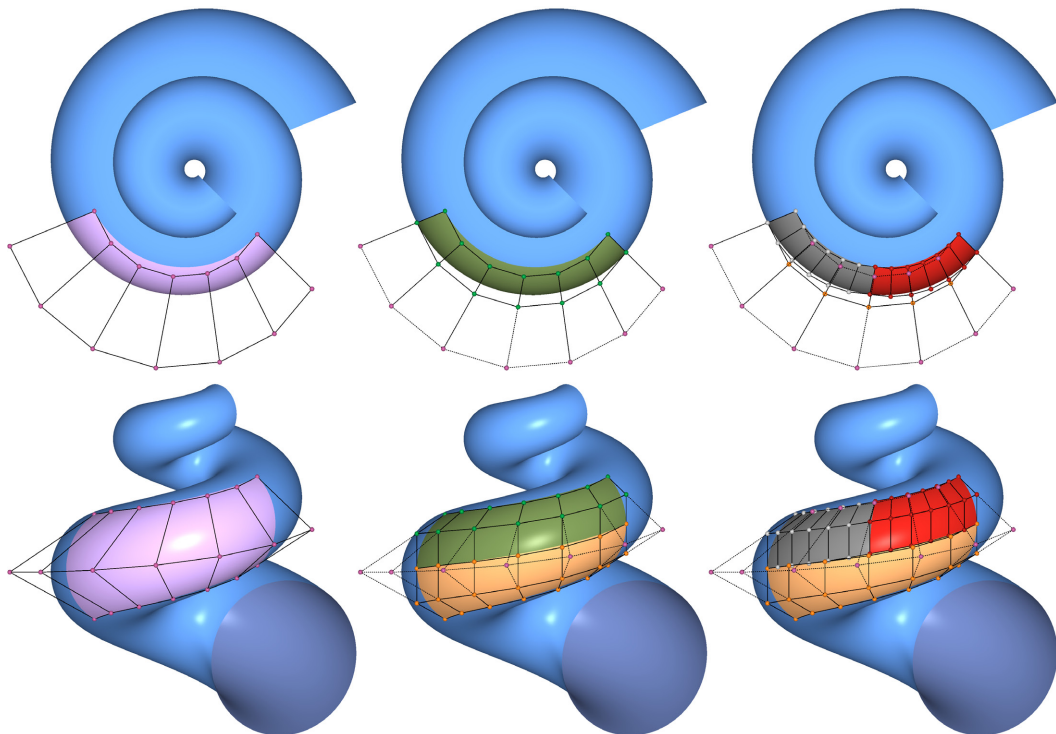
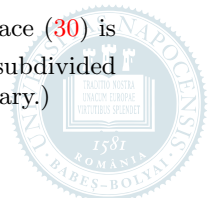


Fig. 4: The surface patch $\mathbf{s}|_{[\frac{11\pi}{2}, \frac{49\pi}{8}] \times [-\frac{\pi}{3}, \frac{\pi}{3}]}$ of the ordinary exponential-trigonometric integral surface (30) is subdivided first at the parameter value $u_1 = 0$, then one of the obtained surface patches is further subdivided at the parameter value $u_0 = \frac{93\pi}{16}$. (All images were rendered by means of the proposed function library.)



2.4 General basis transformation

In [19] we have already constructed the matrix of the general basis transformation that maps the non-negative normalized B-basis $\mathcal{B}_n^{\alpha,\beta}$ to the ordinary basis $\mathcal{F}_n^{\alpha,\beta}$ of the EC space $\mathbb{S}_n^{\alpha,\beta}$. Namely, we have the next theorem.

Theorem 2.4 (General basis transformation, [19]). *The matrix form of the linear transformation that maps the normalized B-basis $\mathcal{B}_n^{\alpha,\beta}$ to the ordinary basis $\mathcal{F}_n^{\alpha,\beta}$ is*

$$[\varphi_{n,i}(u)]_{i=0}^n = [t_{i,j}^n]_{i=0,j=0}^{n,n} \cdot [b_{n,i}(u)]_{i=0}^n, \quad \forall u \in [\alpha, \beta], \quad (43)$$

where $t_{0,j}^n = 1$, $j = 0, 1, \dots, n$ and $t_{i,0}^n = \varphi_{n,i}(\alpha)$, $t_{i,n}^n = \varphi_{n,i}(\beta)$, $i = 0, 1, \dots, n$, while

$$\begin{aligned} t_{i,j}^n &= \varphi_{n,i}(\alpha) - \frac{1}{b_{n,j}^{(j)}(\alpha)} \cdot \sum_{r=1}^{j-1} \frac{\varphi_{n,i}^{(r)}(\alpha)}{b_{n,r}^{(r)}(\alpha)} \left(b_{n,r}^{(j)}(\alpha) + \right. \\ &+ \sum_{\ell=1}^{j-r-1} (-1)^\ell \sum_{r < k_1 < k_2 < \dots < k_\ell < j} \frac{b_{n,r}^{(k_1)}(\alpha) b_{n,k_1}^{(k_2)}(\alpha) b_{n,k_2}^{(k_3)}(\alpha) \dots b_{n,k_{\ell-1}}^{(k_\ell)}(\alpha) b_{n,k_\ell}^{(j)}(\alpha)}{b_{n,k_1}^{(k_1)}(\alpha) b_{n,k_2}^{(k_2)}(\alpha) \dots b_{n,k_\ell}^{(k_\ell)}(\alpha)} \left. \right) + \frac{\varphi_{n,i}^{(j)}(\alpha)}{b_{n,j}^{(j)}(\alpha)}, \\ &i = 1, 2, \dots, n, \quad j = 1, 2, \dots, \left\lfloor \frac{n}{2} \right\rfloor, \end{aligned} \quad (44)$$

$$\begin{aligned} t_{i,n-j}^n &= \varphi_{n,i}(\beta) - \frac{1}{b_{n,n-j}^{(j)}(\beta)} \cdot \sum_{r=1}^{j-1} \frac{\varphi_{n,i}^{(r)}(\beta)}{b_{n,n-r}^{(r)}(\beta)} \left(b_{n,n-r}^{(j)}(\beta) + \right. \\ &+ \sum_{\ell=1}^{j-r-1} (-1)^\ell \sum_{r < k_1 < k_2 < \dots < k_\ell < j} \frac{b_{n,n-r}^{(k_1)}(\beta) b_{n,n-k_1}^{(k_2)}(\beta) b_{n,n-k_2}^{(k_3)}(\beta) \dots b_{n,n-k_{\ell-1}}^{(k_\ell)}(\beta) b_{n,n-k_\ell}^{(j)}(\beta)}{b_{n,n-k_1}^{(k_1)}(\beta) b_{n,n-k_2}^{(k_2)}(\beta) \dots b_{n,n-k_\ell}^{(k_\ell)}(\beta)} \left. \right) \\ &+ \frac{\varphi_{n,i}^{(j)}(\beta)}{b_{n,n-j}^{(j)}(\beta)}, \quad i = 1, 2, \dots, n, \quad j = 1, 2, \dots, \left\lfloor \frac{n}{2} \right\rfloor. \end{aligned} \quad (45)$$

Considering lookup tables that store the zeroth and higher order endpoint derivatives of the bases $\mathcal{F}_n^{\alpha,\beta}$ and $\mathcal{B}_n^{\alpha,\beta}$, we have also investigated the computational complexity (i.e., the number of floating point operations or flops) required for the evaluation of all entries of the general transformation matrix that appears in (43). In [19, Theorem 2.2, p. 45] we have shown that the aforementioned complexity is exponential, but compared with other cubic time numerical algorithms (like function/curve interpolation or least squares approximation techniques based on LU decomposition), the proposed general basis transformation can more efficiently be implemented up to 16-dimensional EC spaces despite the seemingly complicated nature of formulas (44)–(45).

In the next theorem we show that there is even a significantly better way for the evaluation of the matrix of the general basis transformation.

Theorem 2.5 (Efficient general basis transformation). *Using the notations of Theorem 2.4, one has that the non-trivial entries of the matrix $[t_{i,j}^n]_{i=0,j=0}^{n,n}$ of the general basis transformation (43) can be determined by initializing the recursive formulas*

$$t_{i,j}^n = \frac{1}{b_{n,j}^{(j)}(\alpha)} \left(\varphi_{n,i}^{(j)}(\alpha) - \sum_{k=0}^{j-1} t_{i,k}^n b_{n,k}^{(j)}(\alpha) \right), \quad j = 1, \dots, \left\lfloor \frac{n}{2} \right\rfloor, \quad (46)$$

and

$$t_{i,n-j}^n = \frac{1}{b_{n,n-j}^{(j)}(\beta)} \left(\varphi_{n,i}^{(j)}(\beta) - \sum_{k=0}^{j-1} t_{i,n-k}^n b_{n,n-k}^{(j)}(\beta) \right), \quad j = 1, \dots, \left\lfloor \frac{n}{2} \right\rfloor - 1, \quad (47)$$

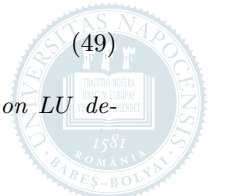
with the starting elements $\{t_{i,0}^n = \varphi_{n,i}(\alpha)\}_{i=1}^n$ and $\{t_{i,n}^n = \varphi_{n,i}(\beta)\}_{i=1}^n$, respectively, for all $i = 1, \dots, n$. Moreover, if the endpoint derivatives $\{\varphi_{n,i}^{(j)}(\alpha), \varphi_{n,i}^{(j)}(\beta), b_{n,i}^{(j)}(\alpha), b_{n,i}^{(j)}(\beta)\}_{i=1, j=0}^{n, \lfloor \frac{n}{2} \rfloor}$ are stored in advance in permanent lookup tables, then the number of flops required by the evaluation of formulas (46) and (47) is the polynomial cost

$$\kappa_{\text{pol}}(n) = \begin{cases} 0, & n = 0, 1, \\ n \cdot \left(\left\lfloor \frac{n}{2} \right\rfloor^2 + 4 \left\lfloor \frac{n}{2} \right\rfloor - 2 \right), & n \geq 2 \end{cases} \quad (48)$$

that is always strictly less than the total cost

$$\kappa_{LU}(n, \delta) = \frac{2}{3}(n+1)^3 - \frac{1}{2}(n+1)^2 - \frac{1}{6}(n+1) + \left(2(n+1)^2 - (n+1) \right) \delta \quad (49)$$

of another numerical δ -dimensional function interpolation or least squares approximation method based on LU decomposition.



Proof. The correctness of formulas (46) and (47) are immediate due to the proof of Theorem 2.4 that can be found in [19, pp. 52–54], where we have used mathematical induction. Formulas (46) and (47) correspond in fact to induction steps based on forward and backward substitutions, the correctness of which were already proved. Final formulas (44) and (45) only give the closed expressions of the patterns that appear after performing all required forward of backward substitutions. Another simple way to verify formulas (46) and (47) is to differentiate the functional equalities

$$\varphi_{n,i}(u) = \sum_{k=0}^n t_{i,k}^n b_{n,k}(u), \quad \forall u \in [\alpha, \beta], \quad i = 1, \dots, n$$

for all orders $j = 1, \dots, \lfloor \frac{n}{2} \rfloor$ at the parameter values $u = \alpha$ and $u = \beta$, respectively, and to apply one of the corresponding endpoint conditions (7)–(8). For example, at $u = \alpha$ one has that

$$\varphi_{n,i}^{(j)}(\alpha) = \sum_{k=0}^n t_{i,k}^n b_{n,k}^{(j)}(\alpha) \stackrel{(7)}{=} \sum_{k=0}^j t_{i,k}^n b_{n,k}^{(j)}(\alpha) = \sum_{k=0}^{j-1} t_{i,k}^n b_{n,k}^{(j)}(\alpha) + t_{i,j}^n b_{n,j}^{(j)}(\alpha),$$

where $b_{n,j}^{(j)}(\alpha) > 0$. Therefore the entry $t_{i,j}^n$ can be obtained by subtraction and division.

Assuming that the endpoint derivatives $\{\varphi_{n,i}^{(j)}(\alpha), \varphi_{n,i}^{(j)}(\beta), b_{n,i}^{(j)}(\alpha), b_{n,i}^{(j)}(\beta)\}_{i=1, j=0}^{n, \lfloor \frac{n}{2} \rfloor}$ are stored in advance in lookup tables, the polynomial computational cost (48) follows from the simplification of the expression

$$n \cdot \left(\sum_{j=1}^{\lfloor \frac{n}{2} \rfloor} (j+2) + \sum_{j=1}^{\lfloor \frac{n}{2} \rfloor - 1} (j+2) \right),$$

where the first and second summations give the number of flops required by the evaluation of the formulas (46) and (47), respectively, while the leading scaling factor n denotes the number of empty non-trivial rows that have to be calculated. At the same time, one can easily prove that $\kappa_{\text{pol}}(n) < \kappa_{LU}(n, \delta)$, $\forall n \geq 0, \delta \geq 1$ and

$$\lim_{n \rightarrow \infty} \frac{\kappa_{\text{pol}}(n)}{\kappa_{LU}(n, \delta)} = \frac{3}{8}. \quad \square$$

Using [19, Corollary 2.1, p. 43], one can also provide ready to use control point configurations for the exact description of those traditional integral parametric curves and (hybrid) surfaces that are specified by coordinate functions given as (products of separable) linear combinations of ordinary basis functions. Namely, by means of general basis transformations, one can implement the control point determining formulas (51) and (53) of the next two theorems.

Theorem 2.6 (Exact description of ordinary integral curves, [19]). *Using EC B-curves of the type (11), the ordinary integral curve*

$$\mathbf{c}(u) = \sum_{i=0}^n \lambda_i \varphi_{n,i}(u), \quad u \in [\alpha, \beta], \quad \lambda_i \in \mathbb{R}^\delta, \quad \delta \geq 2 \quad (50)$$

fulfills the identity

$$\mathbf{c}(u) \equiv \mathbf{c}_n(u) = \sum_{j=0}^n \mathbf{p}_j b_{n,j}(u), \quad \forall u \in [\alpha, \beta],$$

where

$$[\mathbf{p}_0 \ \mathbf{p}_1 \ \dots \ \mathbf{p}_n] = [\lambda_0 \ \lambda_1 \ \dots \ \lambda_n] \cdot [t_{i,j}^n]_{i=0, j=0}^{n, n}. \quad (51)$$

Theorem 2.7 (Exact description of ordinary integral surfaces – extension of Theorem 2.6). *Let*

$$\mathcal{F}_{n_r}^{\alpha_r, \beta_r} = \{\varphi_{n_r, i_r}(u_r) : u_r \in [\alpha_r, \beta_r]\}_{i_r=0}^{n_r}, \quad \varphi_{n_r, 0} \equiv 1$$

be the ordinary basis and

$$\mathcal{B}_{n_r}^{\alpha_r, \beta_r} = \{b_{n_r, j_r}(u_r) : u_r \in [\alpha_r, \beta_r]\}_{j_r=0}^{n_r}$$

be the non-negative normalized B-basis of some EC vector space $\mathbb{S}_{n_r}^{\alpha_r, \beta_r}$ of functions and denote by $[t_{i_r, j_r}^{n_r}]_{i_r=0, j_r=0}^{n_r, n_r}$ the regular square matrix that transforms $\mathcal{B}_{n_r}^{\alpha_r, \beta_r}$ to $\mathcal{F}_{n_r}^{\alpha_r, \beta_r}$, where $r = 0, 1$. Consider also the ordinary integral surface

$$\mathbf{s}(u_0, u_1) = [s^0(u_0, u_1) \ s^1(u_0, u_1) \ s^2(u_0, u_1)]^T \in \mathbb{R}^3, \quad (u_0, u_1) \in [\alpha_0, \beta_0] \times [\alpha_1, \beta_1], \quad (52)$$

where

$$s^\ell(u_0, u_1) = \sum_{\zeta=0}^{\sigma_\ell-1} \prod_{r=0}^1 \left(\sum_{i_r=0}^{n_r} \lambda_{n_r, i_r}^{\ell, \zeta} \varphi_{n_r, i_r}(u_r) \right), \quad \sigma_\ell \geq 1, \quad \ell = 0, 1, 2.$$

Then, by using EC B-surfaces of the type (12), the ordinary surface (52) fulfills the identity

$$\mathbf{s}(u_0, u_1) \equiv \mathbf{s}_{n_0, n_1}(u_0, u_1) = \sum_{j_0=0}^{n_0} \sum_{j_1=0}^{n_1} \mathbf{p}_{j_0, j_1} b_{n_0, j_0}(u_0) b_{n_1, j_1}(u_1), \quad \forall (u_0, u_1) \in [\alpha_0, \beta_0] \times [\alpha_1, \beta_1],$$



where the control points $\mathbf{p}_{j_0, j_1}^\ell = [p_{j_0, j_1}^\ell]_{\ell=0}^2 \in \mathbb{R}^3$ are defined by the coordinates

$$p_{j_0, j_1}^\ell = \sum_{\zeta=0}^{\sigma_\ell-1} \prod_{r=0}^1 \left(\sum_{i_r=0}^{n_r} \lambda_{n_r, i_r}^{\ell, \zeta} t_{i_r, j_r}^{n_r} \right), \quad \ell = 0, 1, 2. \quad (53)$$

Using EC B-curves/surfaces of the type (11)/(12) and applying formulas (51)/(53), the proposed basis transformation can be used for the control point based exact description (or B-representation) of large families of integral or rational ordinary curves/surfaces that may be important in several areas of applied mathematics, since the investigated large class of EC vector spaces also comprise functions that appear in the traditional (or ordinary) parametric description of famous geometric objects like: ellipses; epi- and hypocycloids; epi- and hypotrochoids; Lissajous curves; torus knots; foliums; rose curves; the witch of Agnesi; the cissoid of Diocles; Bernoulli's lemniscate; Zhukovsky airfoil profiles; cycloids; hyperbolas; helices; catenaries; Archimedean and logarithmic spirals; ellipsoids; tori; hyperboloids; catenoids; helicoids; ring, horn and spindle Dupin cyclides; non-orientable surfaces such as Boy's and Steiner's surfaces and the Klein Bottle of Gray.

Figs. 3(a) and 4(b) have already illustrated control point configurations for the B-representation of a single patch of the ordinary exponential-trigonometric integral surface (30). In case of Fig. 5 we have described the entire surface (30) with B-patches of the same order but with varying shape parameters.

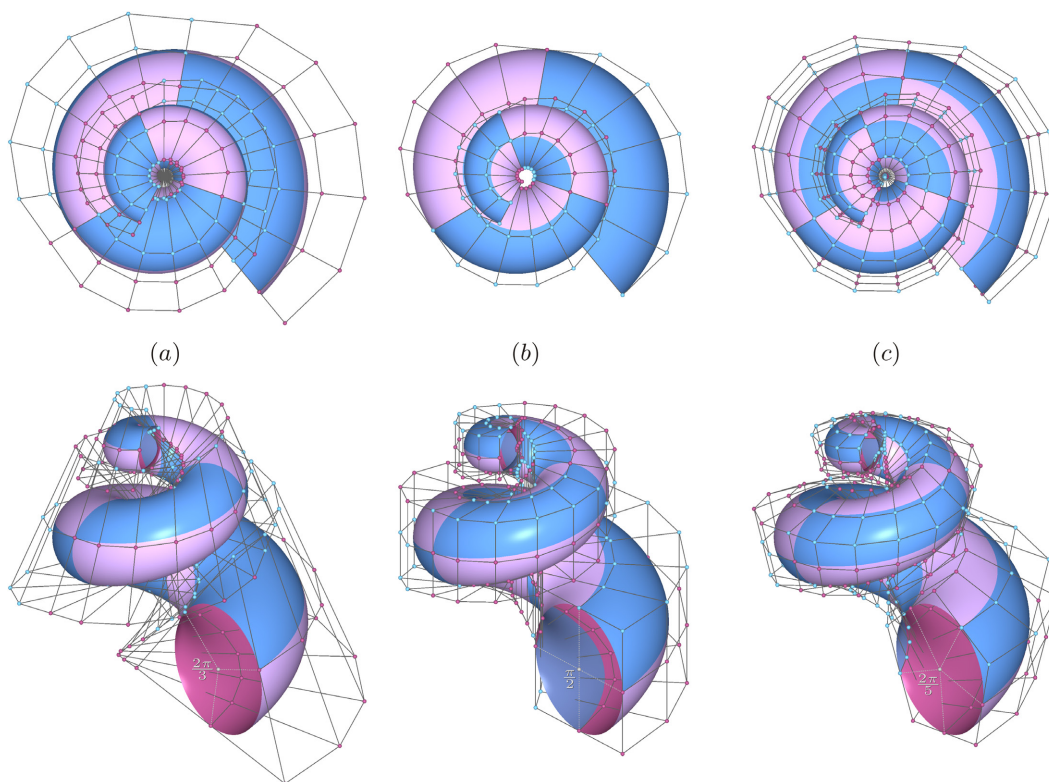


Fig. 5: Different B-representations of the ordinary exponential-trigonometric integral surface (30). Each patch is a B-surface of order $(n_0 = 6, n_1 = 2)$ that is described by means of the non-negative B-bases of the EC spaces $\mathbb{E}\mathbb{T}_6^{\alpha_0, \beta_0}$ and $\mathbb{T}_2^{\alpha_1, \beta_1}$ introduced in Example 2.3, where the definition domain $[\alpha_0, \beta_0] \times [\alpha_1, \beta_1]$ corresponds to pairwise disjunct regions of $[\frac{7\pi}{2}, \frac{49\pi}{8}] \times [-\frac{\pi}{3}, \frac{5\pi}{3}]$. The lengths $\beta_0 - \alpha_0 > 0$ and $\beta_1 - \alpha_1 > 0$ of the varying definition domains can be considered as shape parameters. For example, in cases (a), (b) and (c) the length $\beta_0 - \alpha_0 = \frac{29\pi}{40}$ is fixed, but the length $\beta_1 - \alpha_1$ coincides with the values $\frac{2\pi}{3}$, $\frac{\pi}{2}$ and $\frac{2\pi}{5}$, respectively. (All images were rendered by means of the proposed function library.)

3 Implementation details

Our library assumes that the user has a multi-core CPU and also a GPU that is compatible at least with the desktop variant of OpenGL 3.0. In order to render the geometry, we use vertex buffer objects through the OpenGL Extension Wrangler (GLEW) library¹ and for multi-threading we rely on a C++ compiler that supports at least OpenMP 2.0. Apart from GLEW no other external dependencies are used.

The entire implementation of the proposed function library is explained in the exhaustively commented listings and usage examples of Chapters 2/13–261 and 3/263–326 of the user manual [21] that is included in the

¹ <http://glew.sourceforge.net/>



supplementary material of the manuscript². The tree-view of the header files that can be included from our library is illustrated in Fig. 6.

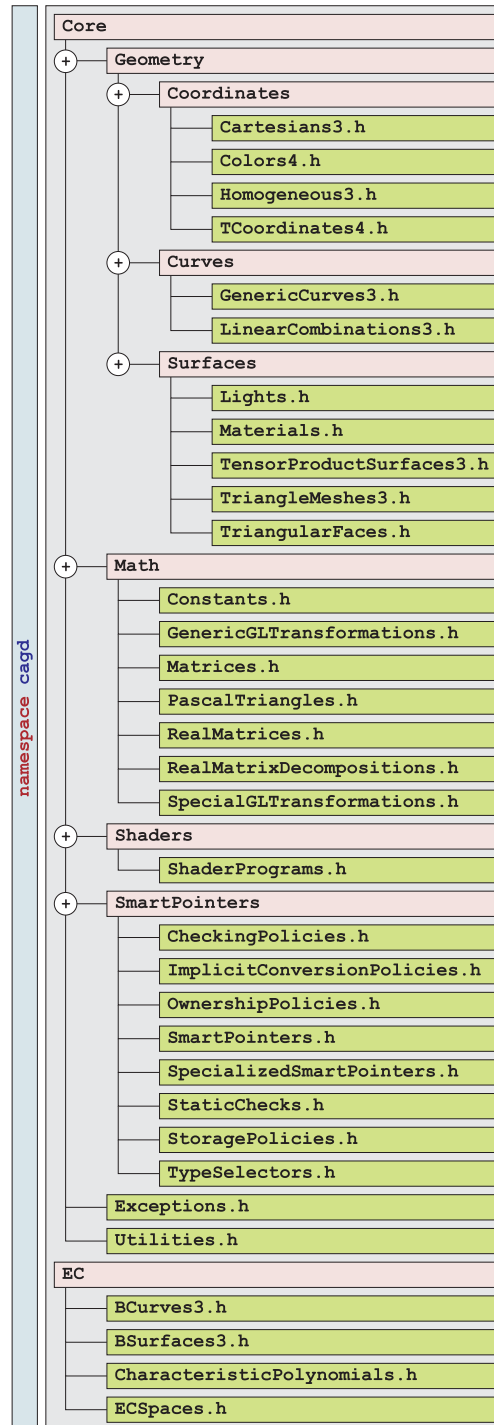
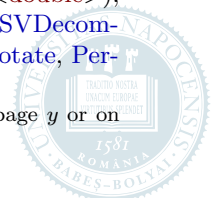


Fig. 6: Tree-view of the header files of the proposed function library

In its current state our library provides two main packages. The first of these is called **Core** and consists of data types that represent:

- exceptions ([Exception](#));
- Cartesian ([Cartesian3](#)), homogeneous ([Homogeneous3](#)) and texture coordinates ([TCoordinate4](#));
- color components ([Color4](#)), different types of lights ([DirectionalLight](#), [PointLight](#), [Spotlight](#)) and materials ([Material](#));
- mathematical constants, generic rectangular ([Matrix<T>](#), [RowMatrix<T>](#), [ColumnMatrix<T>](#)) or triangular template matrices ([TriangularMatrix<T>](#)), real matrices ([RealMatrix: public Matrix<double>](#)), some real matrix decompositions ([PLUDecomposition](#), [FactorizedUnpivotedLUDecomposition](#), [SVDecomposition](#)), generic and derived OpenGL transformations ([GLTransformation](#), [Translate](#), [Scale](#), [Rotate](#), [Per-](#)

² Cross references of the forms x/y and $x/y-z$ show that the referenced object x can be found either on the page y or on pages $y-z$ of the user manual [21].



- perspectiveProjection, OrthogonalProjection, LookAt) and Pascal triangles of binomial coefficients (PascalTriangle: public TriangularMatrix<double>);
- generic and specialized smart pointers (SmartPointer<T,TSP, TOP, TICP, TCP>, SP<T>::DefaultPrimitive, SP<T>::Default, SP<T>::Array, SP<T>::DestructiveCopy, SP<T>::NonIntrusiveReferenceCounting) that provide different storage, ownership, implicit conversion and checking policies (StoragePolicy<T>::Default, StoragePolicy<T>::Array, OwnershipPolicy<T>, ImplicitConversionPolicy, CheckingPolicy<T>::NoCheck, CheckingPolicy<T>::RejectNull, CheckingPolicy<T>::AssertNullDereferenceOrIndirection, CheckingPolicy<T>::AssertNull, CheckingPolicy<T>::AssertNull) in order to avoid memory leaks and to ensure exception safety (one of the most frequently used smart pointers will be the specialized variant SP<T>::Default that ensures default storage and deep copy policies, disallows implicit conversion and rejects null dereference or indirection);
- generic curves (GenericCurve3) and abstract linear combinations (LinearCombination3);
- triangular faces (TriangularFace), simple triangle meshes (TriangleMesh3) and abstract tensor product surfaces (TensorProductSurface3);
- shader programs³ (ShaderProgram) written in the OpenGL Shading Language and used for rendering geometries (like control polygons and nets, or generic curves and triangle meshes obtained e.g. as the images of linear combinations and tensor product surfaces, respectively).

The previously listed classes serve the definition, implementation and testing of the following data types that realize our main objectives and are included in the second main package called **EC**:

- the class **CharacteristicPolynomial** ensures the factorization management and evaluation of characteristic polynomials of type (10);
- EC spaces that comprise the constants and can be identified with the solution spaces of differential equations of type (9) will be instances of the class **ECSpace**;
- EC B-curves of type (11) are represented by the class **BCurve3** that is derived from the abstract base class **LinearCombination3** and is based on the results of Theorems 2.1, 2.2, 2.3, 2.5 and 2.6;
- EC B-surfaces of type (12) are represented by the class **BSurface3** that is a descendant of the abstract base class **TensorProductSurface3** and is based on Theorem 2.7 and on the natural extensions of Theorems 2.1, 2.2 and 2.3.

In what follows, we briefly detail the most important data types of the packages **Core** and **EC**.

3.1 Generic curves

In order to store in vertex buffer objects the points and higher order derivatives of arbitrary smooth parametric (basis) functions, (B-)curves and isoparametric lines of (B-)surfaces, we introduce a class for generic curves (**GenericCurve3**) that will be used for rendering purposes. Its diagram is illustrated in Fig. 7. Apart from vertex buffer object handling methods the class also provides overloaded function operators that can be used for reading or writing the derivatives associated with a curve point. Its definition and full implementation can be found in Listings 2.37/155 and 2.38/157 of [21], respectively.

```

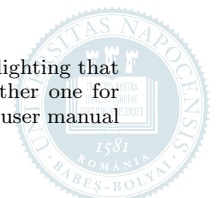
GenericCurve3
<<friend>> LinearCombination3: class
<<friend>> TensorProductSurface3: class
# _usage_flag: GLenum
# _vbo_derivative: RowMatrix<GLuint>
# _derivative: Matrix<Cartesian3>

+ GenericCurve3(maximum_order_of_derivatives: GLint = 2, point_count: GLint = 0,
  usage_flag: GLenum = GL_STATIC_DRAW)
+ GenericCurve3(curve: const GenericCurve3&): GenericCurve3&
+ operator=(rhs: GenericCurve3&): GenericCurve3&
+ deleteVertexBufferObjects(): GLvoid
+ <<const>> renderDerivatives(program: const ShaderProgram&, order: GLint, render_mode: GLenum): GLboolean
+ <<const>> renderDerivatives(order: GLint, render_mode: GLenum,
  vec3_position_location: GLint = 0): GLboolean
+ updateVertexBufferObjects(usage_flag: GLenum = GL_STATIC_DRAW)
+ <<const>> mapDerivatives(order: GLint, access_mode: GLenum = GL_READ_ONLY): GLfloat*
+ <<const>> unmapDerivatives(order: GLint): GLboolean
+ <<const>> operator()(order: GLint, index: GLint): const Cartesian3&
+ operator()(order: GLint, index: GLint): Cartesian3&
+ setDerivative(order: GLint, index: GLint, d: const Cartesian3&): GLboolean
+ setDerivative(order: GLint, index: GLint, x: GLdouble, y: GLdouble, z: GLdouble = 0.0): GLboolean
+ <<const>> derivative(order: GLint, index: GLint, d: Cartesian3&): GLboolean
+ <<const>> derivative(order: GLint, index: GLint, x: GLdouble&, y: GLdouble&, z: GLdouble&): GLboolean
+ <<const>> maximumOrderOfDerivatives(): GLint
+ <<const>> pointCount(): GLint
+ <<const>> usageFlag: GLenum
+ <<const>> clone(): GenericCurve3*
+ ~GenericCurve3()
<<friend>> operator<<(lhs: std::ostream&, rhs: const GenericCurve3&): std::ostream&

```

Fig. 7: Class diagram of generic curves

³ For convenience we have also provided shader programs for simple (flat) color shading, for two-sided per pixel lighting that is able to handle user-defined directional, point and spotlights with uniform front and back materials, and another one for reflection lines that are combined with two-sided per pixel lighting. All figures of the current manuscript and of the user manual [21] were rendered by using these shader programs.



3.2 Simple triangle meshes

We also provide a class for simple triangle meshes ([TriangleMesh3](#)), by means of which one can store in vertex buffer objects the attributes (i.e., position, normal and texture coordinates, color components and connectivity information) of vertices that form the triangular faces of the mesh. The class is also able to load triangulated object file formats and to either map or unmap vertex buffer objects associated with the aforementioned attributes. Its diagram is illustrated in Fig. 8, while its definition and full implementation can be found in Listings 2.40/167 and 2.41/169 of [21], respectively.

```

TriangleMesh3
<<friend>> TensorProductSurface3: class
# _usage_flag: GLenum
# _vbo_positions: GLuint
# _vbo_normals: GLuint
# _vbo_colors: GLuint
# _vbo_tex_coordinates: GLuint
# _vbo_indices: GLuint
# _leftmost_vertex: Cartesian3
# _rightmost_vertex: Cartesian3
# _position: std::vector<Cartesian3>
# _normal: std::vector<Cartesian3>
# _color: std::vector<Color4>
# _tex: std::vector<TCoordinate4>
# _face: std::vector<TriangularFace>

+ TriangleMesh3(vertex_count: GLuint = 0, face_count: GLuint = 0, usage_flag: GLenum = GL_STATIC_DRAW)
+ TriangleMesh3(mesh: const TriangleMesh3&)
+ operator =(rhs: const TriangleMesh3&): TriangleMesh3&
+ deleteVertexBufferObjects(): GLvoid
+ <<const>> render(program: const ShaderProgram&, render_mode: GLenum = GL_TRIANGLES): GLboolean
+ <<const>> render(render_mode: GLenum = GL_TRIANGLES,
vec3_position_location: GLuint = 0,
vec3_normal_location: GLuint = 1,
vec4_color_location: GLuint = 2,
vec4_texture_location: GLuint = 3): GLboolean
+ updateVertexBufferObjects(usage_flag: GLenum = GL_STATIC_DRAW)
+ loadFromOFF(file_name: const std::string&,
translate_and_scale_to_unit_cube: GLboolean = GL_FALSE): GLboolean
+ <<const>> mapPositionBuffer(access_flag: GLenum = GL_READ_ONLY): GLfloat*
+ <<const>> mapNormalBuffer(access_flag: GLenum = GL_READ_ONLY): GLfloat*
+ <<const>> mapColorBuffer(access_flag: GLenum = GL_READ_ONLY): GLfloat*
+ <<const>> mapTextureBuffer(access_flag: GLenum = GL_READ_ONLY): GLfloat*
+ <<const>> unmapVertexBuffer(): GLvoid
+ <<const>> unmapNormalBuffer(): GLvoid
+ <<const>> unmapTextureBuffer(): GLvoid
+ <<const>> vertexCount(): GLuint
+ <<const>> faceCount(): GLuint
+ <<const>> clone(): TriangleMesh3*
+ ~TriangleMesh3()
<<friend>> operator <<(lhs: std::ostream&, rhs: const TriangleMesh3&): std::ostream&
<<friend>> operator >>(lhs: std::istream&, rhs: TriangleMesh3&): std::istream&

```

Fig. 8: Class diagram of simple triangle meshes

3.3 Abstract base classes for linear combinations and tensor product surfaces

We also ensure abstract base classes for arbitrary linear combinations ([LinearCombination3](#)) and tensor product surfaces ([TensorProductSurface3](#)) that are able to generate their images, to update and render their control polygons or nets and to solve curve or surface interpolation problems – provided that the user redeclares and defines in derived classes those pure virtual methods that appear in the interfaces of these abstract classes and are responsible for the evaluation of blending functions and of (partial) derivatives up to a specified maximum order of differentiation. The diagrams of these abstract classes are illustrated in Figs. 9 and 10, while their definitions and full implementations can be found in Listing pairs 2.42/180–2.43/182 and 2.44/188–2.45/192 of [21], respectively.

Pure virtual methods that have to be redeclared and defined in derived classes are [LinearCombination3::blendingFunctionValues](#), [LinearCombination3::calculateDerivatives](#), [TensorProductSurface3::blendingFunctionValues](#), [TensorProductSurface3::calculateAllPartialDerivatives](#) and [TensorProductSurface3::calculateDirectionalDerivatives](#). As we will see, EC B-curves and surfaces of type (11) and (12) will be derived from classes [LinearCombination3](#) and [TensorProductSurface3](#), respectively.

When generating the image of a tensor product surface, the user is also able to choose different color schemes that correspond to the point-wise variations of the x -, y - and z -coordinates, of the length of the normal vectors, of the Gaussian- and mean curvatures, of the Willmore energy and its logarithmic counterpart, of the umbilic deviation and its logarithmic scale, of the total curvature and its logarithmic variant, respectively. (In each case, the applied color map behaves like a temperature variation that ranges from the cold dark blue to the hot red, by passing through the colors cyan, green, yellow and orange such that the minimal and maximal values of a fixed energy type correspond to the extremal colors dark blue and red, respectively. For more details, see Fig. 3.5/311 of [21].)

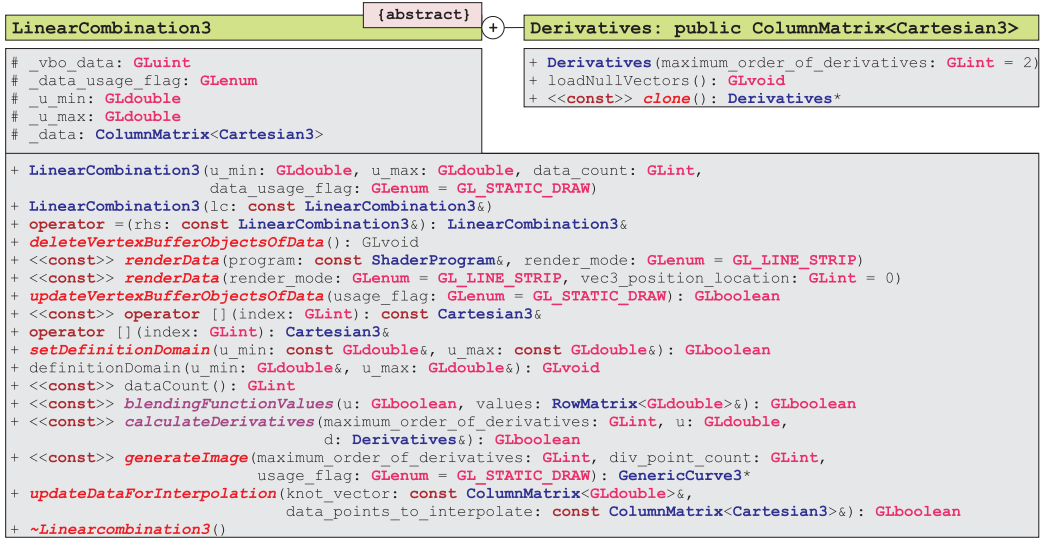


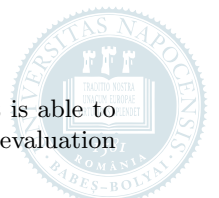
Fig. 9: Class diagram of abstract linear combinations



Fig. 10: Class diagram of abstract tensor product surfaces

3.4 Characteristic polynomials

Characteristic polynomials of type (10) will be instances of the class [CharacteristicPolynomial](#) that is able to store and update the factorization of (10) and also provides an overloaded function operator for evaluation.



purposes. The diagram of the class is illustrated in Fig. 11, while its definition and full implementation can be found in Listings 2.46/206 and 2.47/208 of [21], respectively.

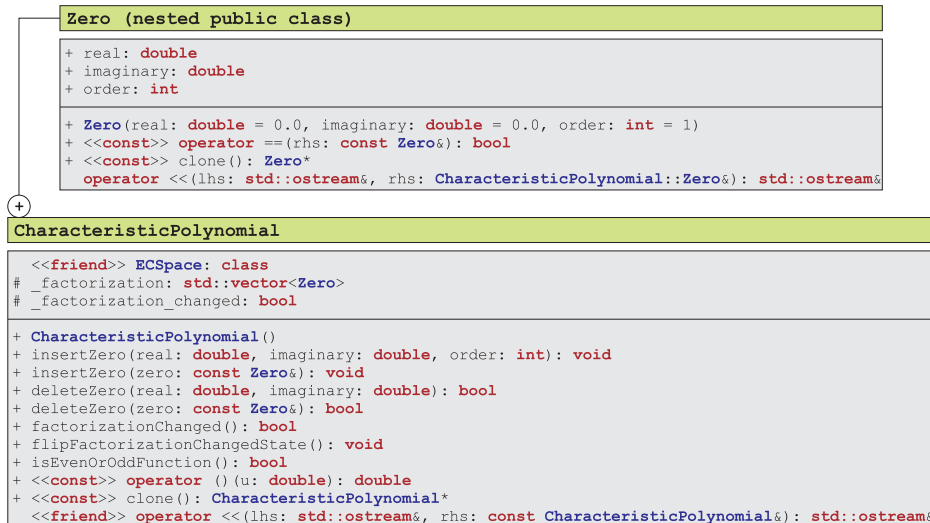


Fig. 11: Class diagram of characteristic polynomials

3.5 EC spaces

EC spaces that comprise the constants and can be identified with the solution spaces of differential equations of type (9) will be instances of the class `ECspace` that

- is able to generate and to update both the ordinary basis and the non-negative normalized B-basis of an EC vector space specified by the factorization of a characteristic polynomial of type (10);
- provides a function operator to evaluate the zeroth and higher order derivatives of both bases at any point of the definition domain;
- can also be used to generate the general basis transformation matrix formulated in Theorem 2.4 that maps the non-negative normalized B-basis to the ordinary basis of the underlying EC space;
- is able to decide whether the specified EC vector is reflection invariant;
- can list the \LaTeX expressions of the ordinary basis functions;
- can also be used to generate the images of both the ordinary basis and the non-negative B-basis functions.

The diagram of the class is illustrated in Fig. 12, while its definition and full implementation can be found in Listings 2.48/211 and 2.49/215, respectively.

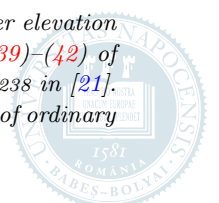
Remark 3.1 (Full implementation details in the user manual). *The construction process (17)–(22) of the non-negative normalized B-basis functions of the underlying EC space and their differentiation formulas (23) are implemented in lines 570/225–812/228 and 837/229–914/230 of Listing 2.49/215 in [21], respectively. Formulas (46)–(47) of the general basis transformation are implemented in lines 919/230–986/231 of Listing 2.49/215 in [21].*

Remark 3.2 (Examples in the user manual). *Deriving from the base class `ECspace`, one can define special (like pure polynomial/trigonometric/hyperbolic and mixed exponential-trigonometric or algebraic- $\{\text{trigonometric/hyperbolic/exponential-trigonometric}\}$) EC spaces as it is presented by several examples in Listings 3.1/264 and 3.2/266 of [21]. In Listings 3.10/282 and 3.11/283 of [21], we also provided examples for the evaluation, differentiation and rendering of both the ordinary basis and the non-negative normalized B-basis of different types of EC spaces.*

3.6 EC B-curves

EC B-curves of type (11) are represented by the class `BCurve3` that is derived from the abstract base class `LinearCombination3` and is based on the results of Theorems 2.1, 2.2, 2.3, 2.5 and 2.6. It can be used to perform general order elevation, subdivision and to exactly describe user-specified ordinary integral curves by means of convex combinations of control points and non-negative normalized B-basis functions. The diagram of the class is illustrated in Fig. 13, while its definition and full implementation can be found in Listings 2.50/236 and 2.51/238 of [21], respectively. Note that the class redeclares and defines those pure virtual methods that are inherited as interfaces from the abstract base class `LinearCombination3`.

Remark 3.3 (Full implementation details in the user manual). *Formulas (28)–(29) of the general order elevation stated in Theorem 2.2 are implemented in lines 137/241–160/241 of Listing 2.51/238 in [21]. Formulas (39)–(42) of the general B-algorithm stated in Theorem 2.3 are implemented in lines 199/242–322/244 of Listing 2.51/238 in [21]. Using EC B-curves of type (11) and formula (51) of Theorem 2.6, the control point based exact description of ordinary integral curves of type (50) is implemented in lines 349/244–374/245 of Listing 2.51/238 in [21].*



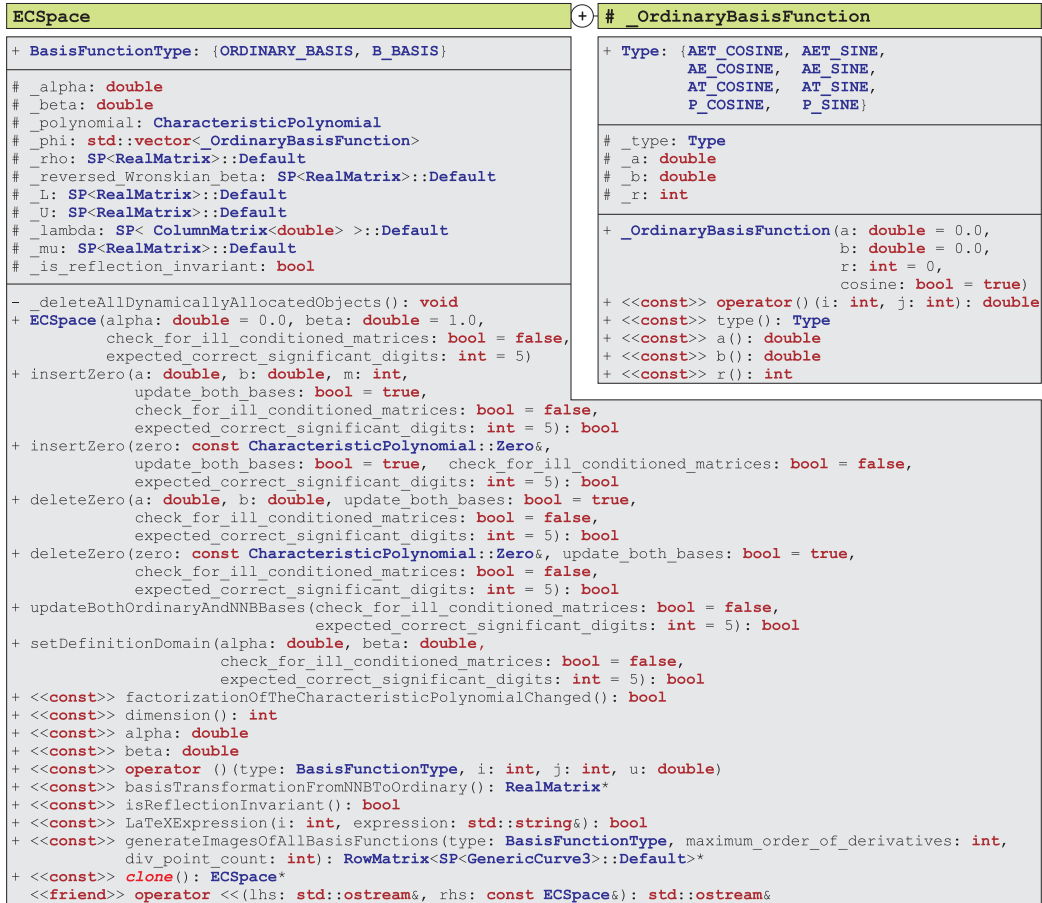


Fig. 12: Class diagram of a translation invariant extended Chebyshev spaces that can be identified with the solution space of a constant-coefficient homogeneous linear differential equation

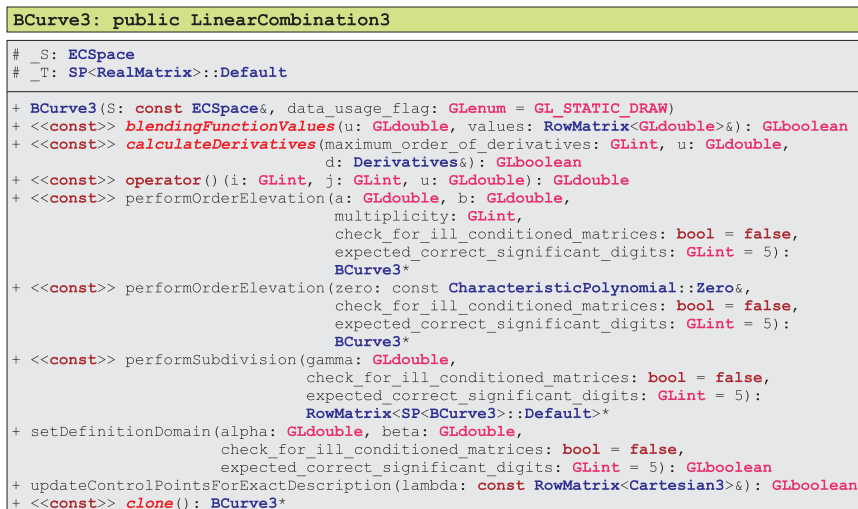
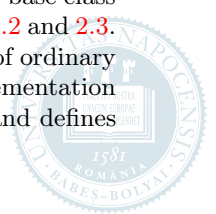


Fig. 13: Class diagram of general EC B-curves

Remark 3.4 (Examples in the user manual). Listings 3.12/286–3.13/287 and Fig. 3.2/293 of [21] provide examples for the definition, generation, evaluation, differentiation, order elevation, subdivision and rendering of different types of B-curves. Listings 3.14/293–3.15/294 and Fig. 3.3/298 of [21] provide an example for the control point based exact description (or B-representation) of integral curves given in traditional (i.e., ordinary) parametric form.

3.7 EC B-surfaces

EC B-surfaces of type (12) are represented by the class `BSurface3` that is a descendant of the abstract base class `TensorProductSurface3` and is based on Theorem 2.7 and on the natural extensions of Theorems 2.1, 2.2 and 2.3. It can be used to perform general order elevation, subdivision and to describe exactly a large family of ordinary integral surfaces of type (52). Its diagram is presented in Fig. 14, while its definition and full implementation can be found in Listings 2.52/246 and 2.53/248 of [21], respectively. Note that the class redeclares and defines those pure virtual methods that are inherited from the abstract base class `TensorProductSurface3`.



```

OrdinarySurfaceCoefficients
# _lambda: std::vector< std::vector< pair< RowMatrix<GLdouble>, RowMatrix<GLdouble> > > >
+ OrdinarySurfaceCoefficients(u_dimension: GLint, v_dimension: GLint, sigma: const std::vector<GLint>&)
+ <<const>> operator()(ell: GLint, zeta: GLint, type: variable::Type, index: GLint): GLdouble
+ operator()(ell: GLint, zeta: GLint, type: variable::Type, index: GLint): GLdouble&
+ <<const>> sigma(ell: GLint): GLint
+ <<const>> dimension(type: variable::Type): GLint
+ <<const>> clone(): OrdinarySurfaceCoefficients*

BSurface3: public TensorProductSurface3
# _S: ECspace[2]
# _T: SP<RealSquareMatrix>::Default[2]
+ BSurface3(u_space: const ECspace&, v_space: const ECspace&)
+ setInterval(type: variable::Type, alpha: GLdouble, beta: GLdouble,
  check_for_ill_conditioned_matrices: bool = false,
  expected_correct_significant_digits: GLint = 5): GLboolean
+ <<const>> blendingFunctionValues(type: variable::Type, parameter_value: GLdouble,
  values: RowMatrix<GLdouble>&): GLboolean
+ <<const>> calculateAllPartialDerivatives(maximum_order_of_derivatives: GLint,
  u: GLdouble, v: GLdouble, pd: PartialDerivatives&): GLboolean
+ <<const>> calculateDirectionalDerivatives(direction: variable::Type,
  maximum_order_of_derivatives: GLint,
  u: GLdouble, v: GLdouble, v,
  d: DirectionalDerivatives&): GLboolean
+ <<const>> operator()(type: variable::Type, i: GLint, j: GLint, parameter_value: GLdouble): GLdouble
+ <<const>> performOrderElevation(type: variable::Type, a: GLdouble, b: GLdouble, order: GLint,
  check_for_ill_conditioned_matrices: bool = false,
  expected_correct_significant_digits: GLint = 5): BSurface3*
+ <<const>> performOrderElevation(type: variable::Type, zero: const CharacteristicPolynomial::Zero&,
  check_for_ill_conditioned_matrices: bool = false,
  expected_correct_significant_digits: GLint = 5): BSurface3*
+ <<const>> performSubdivision(type: variable::Type, gamma: GLdouble,
  check_for_ill_conditioned_matrices: bool = false,
  expected_correct_significant_digits: GLint = 5):
  RowMatrix<SP<BSurface3>::Default>*
+ updateControlPointsForExactDescription(lambda: const OrdinarySurfaceCoefficients&): GLboolean
+ <<const>> clone(): BSurface3*

```

Fig. 14: Class diagrams of general EC B-surfaces and of ordinary surface coefficients

Remark 3.5 (Full implementation details in the user manual). *The results of Theorem 2.2 can also be extended to the general order elevation of EC B-surfaces of type (12) and our function library ensures this possibility as well: the order elevation of B-surfaces is implemented in lines 282/252–501/256 of Listing 2.53/248 in [21]. The subdivision technique presented in Theorem 2.3 can also be extended to EC B-surfaces as it is implemented in lines 507/256–767/260 of Listing 2.53/248 in [21]. Using EC B-surfaces of type (12) and formula (53) of Theorem 2.7, the control point based exact description (or B-representation) of ordinary integral surfaces of type (52) is implemented in lines 773/260–812/261 of Listing 2.53/248 in [21].*

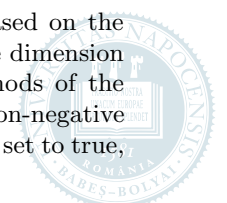
Remark 3.6 (Examples in the user manual). *Listings 3.16/297–3.17/299 and Figs. 3.4/310–3.7/313 of [21] provide examples for the definition, generation, evaluation, differentiation, order elevation, subdivision and rendering of different types of B-surfaces. Listings 3.18/314–3.19/315 and Figs. 3.8/326– 3.9/326 of [21] give examples for the control point based exact description (or B-representation) of integral surfaces given in traditional (i.e., ordinary) parametric form and for the generation, evaluation, differentiation and rendering of isoparametric lines of B-surfaces.*

4 Further examples, run-time statistics and handling possible numerical instabilities

We have seen that each of the proposed algorithms relies on the successful evaluation of zeroth and higher order (endpoint) derivatives of either of the ordinary basis functions (1) or of the non-negative normalized B-basis (4). The order of (endpoint) derivatives that have to be evaluated increases proportionally with the dimension of the underlying EC space. Due to floating point arithmetical operations, the maximal dimension for which one does not bump into numerical instabilities depends both on the endpoints of the definition domain and on the type of the ordinary basis functions of the given EC space – depending on the case, it may be smaller or greater, but considering that, in practice, curves and surfaces are mostly composed of smoothly joined lower order arcs and patches, we think that the proposed algorithms can be useful in case of real-life applications. In order to empirically underpin these statements, here we present several run-time statistics and we also describe how to detect and handle possible numerical instabilities. Using the Microsoft Visual Studio Compiler 15.0, we have tested the 64-bit release version of our library both on an affordable laptop with an Intel[®] Core™ i7-3720QM CPU₁ @ 2.60 GHz (4 cores, 8 threads) and an nVidia GPU₁ GeForce GT 650M and on a desktop computer with an Intel[®] Xeon[®] E5-2670 CPU₂ @ 2.60 GHz (8 cores, 16 threads) and an nVidia GPU₂ GeForce GTX 680.

4.1 Determining the maximum dimension

The construction process (17)–(22) of the non-negative normalized B-basis of an EC space is based on the solution of several systems of linear equations that may be ill-conditioned either for relatively large dimension numbers or for poorly selected endpoints of the definition domain. For this reason several methods of the proposed function library expect a boolean flag named “check_for_ill_conditioned_matrices” and a non-negative integer called “expected_correct_significant_digits”. If the flag “check_for_ill_conditioned_matrices” is set to true,



these methods will calculate the condition number of each matrix that appears in the construction process (17)–(22). Using singular value decomposition [18], each condition number is determined as the ratio of the largest and smallest singular values of the corresponding matrices. If at least one of the obtained condition numbers is too large, i.e., when the number of estimated correct significant digits is less than the number of expected ones, these methods will throw an exception that one of the systems of linear equations is ill-conditioned and therefore its solution may be inaccurate. If the user catches such an exception, one can try:

- to lower the number of expected correct significant digits;
- to decrease the dimension of the underlying EC space;
- to change the endpoints of the definition domain $[\alpha, \beta]$;
- to run the code without testing for ill-conditioned matrices and hope for the best.

Note that in certain cases the standard condition number may lead to an overly pessimistic estimate for the overall error and at the same time, by activating the boolean flag “check_for_ill_conditioned_matrices”, the run-time of the aforementioned methods will increase. Several numerical tests show that ill-conditioned matrices appear during the construction process (17)–(22) when one tries to define EC spaces with relatively big dimensions. Considering that, in practice, (spline) curves and surfaces are mostly described by basis functions of lower dimensional vector spaces, by default we opted for speed, i.e., initially the flag “check_for_ill_conditioned_matrices” is set to false. Naturally, if one obtains mathematically or geometrically unexpected results (that violate either the convex hull or variation diminishing properties, or they are simply meaninglessly noisy and chaotic), then one should (also) study the values of the condition numbers mentioned above.

The maximal dimension for which one does not bump into numerical instabilities also depends on possible operations that have to be performed on the obtained B-curves/surfaces. If one only intends to evaluate, (partially) differentiate and render B-curves/surfaces without performing order elevations, subdivisions or B-representations on them, the dimensions of the applied EC spaces can be bigger than otherwise. The reason of this is that differentiations and arithmetical floating point operations that appear in formulas of Theorems 2.2, 2.3 and 2.5 further increase the accumulated numerical errors that causes the quicker disappearance of the correct digits.

Consider the polynomial, trigonometric, hyperbolic, algebraic-trigonometric and algebraic-exponential-trigonometric EC spaces

$$\mathbb{P}_n^{0,1} := \langle \overline{\mathcal{P}}_n^{0,1} \rangle := \langle \{1, u, \dots, u^n : u \in [0, 1]\} \rangle, \quad \dim \mathbb{P}_n^{0,1} = n + 1, \quad (54)$$

$$\mathbb{T}_{2n}^{0, \frac{\pi}{2}} := \langle \overline{\mathcal{T}}_{2n}^{0, \frac{\pi}{2}} \rangle := \langle \{1, \cos(u), \sin(u), \dots, \cos(nu), \sin(nu) : u \in [0, \pi/2]\} \rangle, \quad (55)$$

$$\dim \mathbb{T}_{2n}^{0, \frac{\pi}{2}} = 2n + 1,$$

$$\mathbb{H}_{2n}^{0, \pi} := \langle \overline{\mathcal{H}}_{2n}^{0, \pi} \rangle := \langle \{1, \cosh(u), \sinh(u), \dots, \cosh(nu), \sinh(nu) : u \in [0, \pi]\} \rangle, \quad (56)$$

$$\dim \mathbb{H}_{2n}^{0, \pi} = 2n + 1,$$

$$\mathbb{A}\mathbb{T}_{n(n+2)}^{0, 2\pi} := \langle \overline{\mathcal{A}\mathcal{T}}_{n(n+2)}^{0, 2\pi} \rangle := \left\langle \left\{ 1, u, \dots, u^n, \{u^r \cos(ku), u^r \sin(ku)\}_{r=0, k=1}^{n-k, n} : u \in [0, 2\pi] \right\} \right\rangle, \quad (57)$$

$$\dim \mathbb{A}\mathbb{T}_{n(n+2)}^{0, 2\pi} = (n + 1)^2$$

and

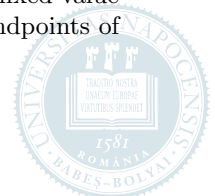
$$\mathbb{A}\mathbb{E}\mathbb{T}_{n(2n+3)}^{-\frac{3\pi}{4}, \frac{3\pi}{4}} := \langle \overline{\mathcal{A}\mathcal{E}\mathcal{T}}_{n(2n+3)}^{-\frac{3\pi}{4}, \frac{3\pi}{4}} \rangle := \left\langle \left\{ 1, u, \dots, u^n, \{u^r \cos(ku), u^r \sin(ku)\}_{r=0, k=1}^{n-k, n}, \{u^r \cosh(ku), u^r \sinh(ku)\}_{r=0, k=1}^{n-k, n} : u \in [-3\pi/4, 3\pi/4] \right\} \right\rangle, \quad (58)$$

$$\dim \mathbb{A}\mathbb{T}_{n(2n+3)}^{-\frac{3\pi}{4}, \frac{3\pi}{4}} = 2n^2 + 3n + 1,$$

respectively. Assuming that the user tries to model B-curves/surfaces without performing order elevations, subdivision and B-representations on them, Fig. 15 illustrates in horizontal direction the maximal values of n for which one does not enter into numerical instabilities in spite of the fact that these values are greater than those for which the estimated number of correct digits would equal to only 1 based on the detected corresponding maximal condition numbers and on the machine epsilon $\varepsilon \approx 2.220446 \cdot 10^{-16}$ of double precision types. The latter values of n are highlighted with the tipping points of the tick vertical dashed lines with arrows pointing to their left and right sides.

Fig. 15 also shows in vertical direction confidence intervals for the unknown theoretical mean value of the time (measured in milliseconds) that is required to calculate all information needed for the evaluation and differentiation of both the ordinary basis and the non-negative normalized B-basis of the given EC spaces for each value of n . The run-time related confidence intervals were determined as follows. Consider the fixed significance level $s = 0.01$ and let $N = 1000$ be a fixed number of independent trials for each values of n . Assuming that $[\tau_i^n]_{i=1}^N$ is the elapsed time sample obtained by repeatedly testing an algorithm for a fixed value of n and denoting by $F_{S(N-1)}$ Student’s T-distribution function of $N - 1$ degrees of freedom, the endpoints of the confidence intervals were computed as

$$(\tau_{\min}^n, \tau_{\max}^n) = \left(\max \left\{ \bar{\tau}_n - \frac{\bar{\sigma}_n}{\sqrt{N}} \cdot x_{1-\frac{s}{2}, N-1}, 0 \right\}, \bar{\tau}_n + \frac{\bar{\sigma}_n}{\sqrt{N}} \cdot x_{1-\frac{s}{2}, N-1} \right),$$



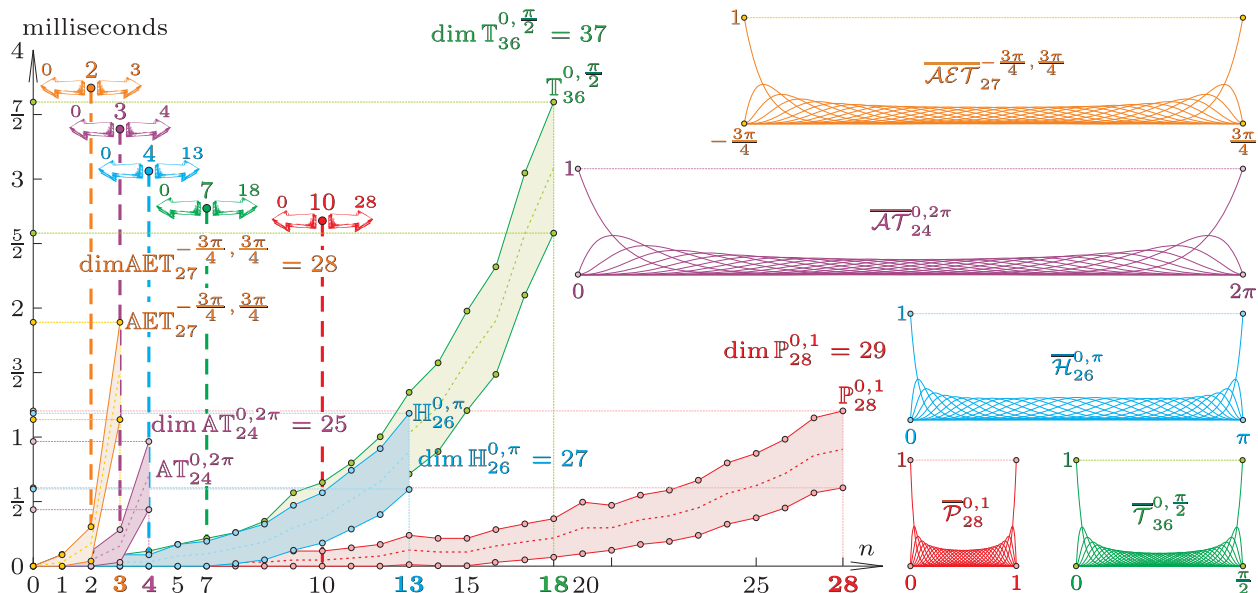


Fig. 15: Maximal dimensions for which one does not bump into numerical instabilities in case of B-curve/surface generation and differentiation in EC spaces (54), (55), (56), (57) and (58). The lower and upper boundary of the shaded regions correspond to the endpoints of confidence intervals that include the unknown theoretical mean value of the time (measured in milliseconds on CPU₁) that is required to construct all data needed for the evaluation and differentiation of both the ordinary basis and the non-negative normalized B-basis of the given EC spaces for each value of n . (The dotted centerlines of the shaded areas interpolate the sample mean of the elapsed time values.) The tipping points of the thick vertical dashed lines (with arrows pointing to their left and right sides) highlight those values of n for which the estimated number of correct digits would equal to only 1 based on the detected corresponding maximal condition numbers.

where

$$\bar{\tau}_n = \frac{1}{N} \sum_{i=1}^N \tau_i^n, \quad \bar{\sigma}_n = \sqrt{\frac{1}{N-1} \sum_{i=1}^N (\tau_i^n - \bar{\tau}_n)^2}, \quad x_{1-\frac{s}{2}, N-1} = F_{S(N-1)}^{-1} \left(1 - \frac{s}{2} \right).$$

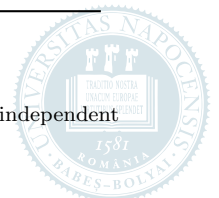
If one also intends to perform special operations (like subdivision or order elevation) on B-curves/surfaces constructed in EC spaces (54)–(58), usually one should work with numbers n that are smaller than or equal to those values that are highlighted by the tipping points of the thick vertical dashed lines of Fig. 15. (In order to avoid badly scaled or close to singular matrices that may appear in the B-basis construction process (17)–(22) during repeated subdivisions, usually the dimension of the underlying EC space should be decreased proportionally to the shrinking length of the definition domain.)

Table 1 provides run-time statistics for the differentiation of those non-negative B-basis functions that are illustrated in Fig. 15. (Note that, in practice, is highly unlikely that one would use as many basis functions as shown in Fig. 15 in order to describe arcs and patches of composite curves and surfaces, respectively. Here we tried to push the boundaries of the proposed function library in some cases that may also appear in real-world applications. In lower dimensional EC spaces, the endpoints of run-time related confidence intervals will be significantly smaller.)

Table 1: Run-time statistics of non-negative B-basis function differentiation up to a given maximal order

Task: multi-threaded differentiation of all functions of a specific non-negative normalized B-basis at 100 uniform subdivision points from order 0 up to a maximal order d_{\max}	Run-time related confidence intervals ⁴
$\bar{\mathcal{P}}_{28}^{0,1}, d_{\max} = \left\lfloor \frac{1}{2} \dim \mathbb{P}_{28}^{0,1} \right\rfloor = 14$	$(91.105, 93.887)_{\text{CPU}_1}$; $(49.676, 51.288)_{\text{CPU}_2}$
$\bar{\mathcal{T}}_{36}^{0, \frac{\pi}{2}}, d_{\max} = \left\lfloor \frac{1}{2} \dim \mathbb{T}_{36}^{0, \frac{\pi}{2}} \right\rfloor = 18$	$(423.504, 431.568)_{\text{CPU}_1}$; $(217.626, 220.150)_{\text{CPU}_2}$
$\bar{\mathcal{H}}_{26}^{0, \pi}, d_{\max} = \left\lfloor \frac{1}{2} \dim \mathbb{H}_{26}^{0, \pi} \right\rfloor = 13$	$(86.4903, 88.9317)_{\text{CPU}_1}$; $(46.1756, 48.8821)_{\text{CPU}_2}$
$\bar{\mathcal{A}}_{24}^{0, 2\pi}, d_{\max} = \left\lfloor \frac{1}{2} \dim \mathbb{A}_{24}^{0, 2\pi} \right\rfloor = 12$	$(75.4589, 77.7331)_{\text{CPU}_1}$; $(42.9555, 44.7865)_{\text{CPU}_2}$
$\bar{\mathcal{AET}}_{27}^{-\frac{3\pi}{4}, \frac{3\pi}{4}}, d_{\max} = \left\lfloor \frac{1}{2} \dim \mathbb{AET}_{27}^{-\frac{3\pi}{4}, \frac{3\pi}{4}} \right\rfloor = 14$	$(257.381, 262.379)_{\text{CPU}_1}$; $(133.511, 135.691)_{\text{CPU}_2}$

⁴ The endpoints are measured in milliseconds and are calculated by using Student's T-distribution with 1000 independent trials at the fixed significance level 0.01.



Apart from possibly incorrect order elevation and subdivision, too big dimension numbers will generate undesired point-wise perturbations in the shapes of the generated B-basis functions and these numerical instabilities will also be inherited by the shapes of B-curves/surfaces in the form of unwanted undulations. Since there are infinitely many EC spaces with a vast possibility of inner structure, we cannot give a general recipe for the critical maximal dimension number for which the outputs of the proposed algorithms are correct – *its value should be determined empirically by the user*. Given a user-defined instance of the class `ECSpace`, the proposed function library is able to generate and render the shape of the non-negative normalized B-basis functions by using the methods `ECSpace::generateImagesOfAllBasisFunctions`, `GenericCurve3::updateVertexBufferObjects` and `GenericCurve3::renderDerivatives` (for more details consider e.g. Listings 3.1/263–3.2/266 and 3.10/282–3.11/283 of [21]). If in case of an `ECSpace` object one obtains an image similar to Fig. 16(b) or even a more drastic one from the perspective of the undesired error suggesting point-wise perturbations, then one can conclude that the dimension of the constructed EC space is too big. If this is the case, one may try to translate or decrease the length of the definition domain (since its endpoints have a significant effect on the endpoint derivatives that are required by all algorithms), or if this does not remedy the situation then one has to exclude some of the ordinary basis functions that span the initial space.

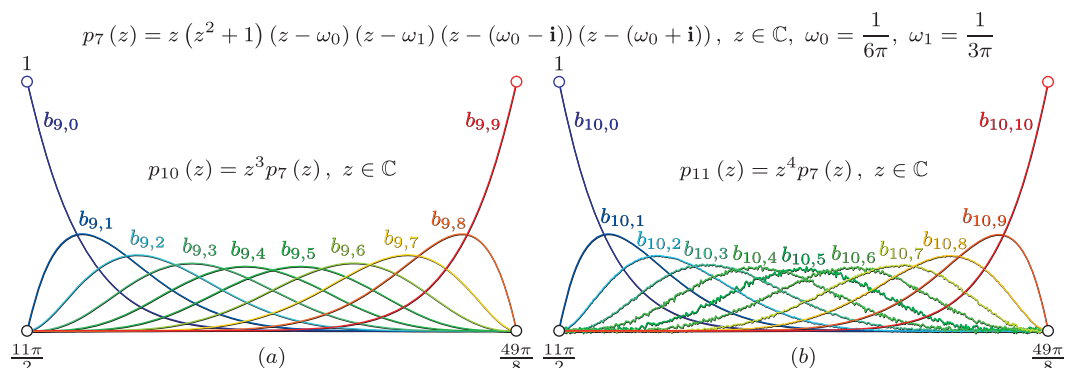
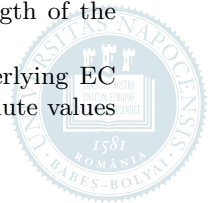


Fig. 16: The characteristic polynomial p_7 and the definition domain $[\alpha, \beta] = [\frac{11\pi}{2}, \frac{49\pi}{8}]$ are the same as in Example 2.3 that introduced the exponential-trigonometric EC space $\mathbb{ET}_6^{\alpha, \beta}$. In cases (a) and (b) of the figure we have created two new algebraic-exponential-trigonometric EC spaces from $\mathbb{ET}_6^{\alpha, \beta}$, by increasing the multiplicity of the zero $z = 0$ of p_7 from 1 to 3 and 4, respectively. Observe that in case (b) the method which should generate the non-negative normalized B-basis becomes numerically unstable, i.e., over the given definition domain the dimension of the initial EC space $\mathbb{ET}_6^{\alpha, \beta}$ should be increased from 7 only up to 10, by appending its ordinary basis with the monomials $\{u, u^2 : u \in [\alpha, \beta]\}$. (If one defines the initial space on a different domain or appends its ordinary basis with other linearly independent functions, the maximum dimension may differ from the previously determined 10.)

4.2 Determining the length of the definition domain

The length $\beta - \alpha > 0$ of the definition domain $[\alpha, \beta]$ should be strictly less than the critical length (21) of the underlying EC space $\mathbb{S}_n^{\alpha, \beta}$, otherwise the given space may not provide shape preserving representations, e.g. the generated “B-basis” functions may not form a strictly totally positive function system that usually leads to the violation of the convex hull and variation diminishing properties of the induced “B-curves”. This property is related to the fact that the space of derivatives fails to be EC for too large intervals [1] (leading to the idea of the critical length of a space of functions that is invariant under translations). There are some types of translation invariant EC spaces in case of which we know the explicit values of the corresponding critical lengths, e.g. in [22] it is proved that in case of the vector space of trigonometric polynomials of order at most n (or of degree at most $2n$) the length of the definition domain should be less than π , in [23] appears that in case of the vector space of hyperbolic polynomials of order at most n (or degree $2n$) the length of the definition domain can be any positive real number, and in case of a special algebraic-trigonometric (or cycloidal) vector space detailed in [1, 3] the value of the critical length is determined by using a constructive numerical procedure. However, in general, the exact determination or at least the approximation of the critical length of a vector space – as the supremum of the lengths of the intervals on which the given space is EC – is not a trivial problem. Therefore, when one creates an instance of the class `ECSpace` that has not been previously studied in the literature, we advise to always check whether each generated B-basis function is indeed non-negative over the user-defined definition domain. If there are subregions on which at least a function becomes negative, the length of the definition domain should be decreased and the verifying test should be repeated.

Numerical instabilities may also appear when the length of the definition domain of the underlying EC space is too small, since this may lead both to higher order endpoint derivatives with too big absolute values and to almost singular or badly scaled systems of linear equations.



As one can see, the length of the definition domain influences both the correctness and the numerical stability of all proposed algorithms. As a golden rule, the user should avoid the usage of either too large or too small definition domains.

4.3 Further examples and run-time statistics

The proposed library is also able to evaluate and render the zeroth and higher order derivatives of B-curves and of isoparametric lines of B-surfaces as it is illustrated in Fig. 17.

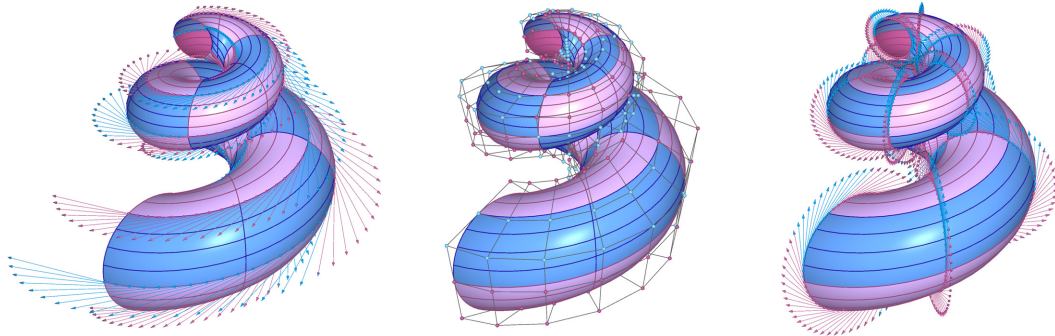


Fig. 17: Isoparametric lines and their first order derivatives in case of a possible B-representation of the ordinary exponential-trigonometric integral surface (30). (The illustrated B-surface patches coincide with those in Fig. 5(c). Along all 25 B-surface patches we have generated 5 and 3 isoparametric lines in directions u_0 and u_1 of the definition domains, respectively. The u_0 - and u_1 -isoparametric lines consist of 20 and 13 subdivision points, respectively. For better visibility, we have rendered the tangent vectors only of some of the isoparametric lines.)

Note that, by using the control point based exact description methods proposed in Theorems 2.6 and 2.7, theoretically one can provide infinitely order of precision concerning the zeroth and higher order (partial) derivatives. Apart from rational polynomial curves and surfaces, this cannot be achieved by the standard rational Bézier or NURBS curve and surface modeling tools (e.g. elliptic or hyperbolic arcs of conic sections can be described as rational Bézier curves, but these will provide neither natural parametrization nor higher order precision concerning the derivatives). Moreover, these standard rational polynomial models cannot encompass transcendental curves and surfaces and they also rely on special non-negative weight vectors/matrices of rank at least 1 – the calculation of which, apart from some simple cases, is cumbersome for the designer.

Table 2 provides further run-time related confidence intervals that were obtained in case of the remaining examples presented by the manuscript.

5 Closure

Using the unique non-negative normalized B-bases of EC spaces that comprise the constants and can be identified with the translation invariant solution spaces of constant-coefficient homogeneous linear differential equations, we have proposed a platform-independent OpenGL and C++ based multi-threaded robust and flexible function library for control point based curve and surface modeling. The proposed data structures are able to generate, differentiate and render both the ordinary basis and the non-negative normalized B-basis of the underlying EC spaces. Our library can also create, (partially) differentiate, modify and render a large family of EC B-curves and tensor product B-surfaces and is also able to perform operations (like order elevation and subdivision) on them (at least up to a reasonable number of dimension and with acceptable numerical precision). The user also has the possibility to describe exactly arbitrary ordinary integral curves and surfaces by means of B-curves and B-surfaces, respectively. We also provide methods for the solution of B-curve and B-surface interpolation problems.

We think, in Subsection 1.1 we have provided sufficient motivations and advantages both for the usage of not necessarily polynomial non-negative B-basis functions and for the application of B-curves/surfaces implied by them. Moreover, as it is suggested by the included run-time statistics, the proposed function library is quite responsive and reliable even on an affordable laptop that has a multi-core CPU and a dedicated GPU that is compatible at least with the desktop variant of OpenGL 3.0.

We deliberately chose the surface (30) in case of Figs. 3, 4, 5 and 17, since it is a transcendental surface that cannot exactly be described by means of the standard (rational) Bézier and (non-uniform) B-spline modeling

⁵ The endpoints are measured in milliseconds and are calculated by using Student's T-distribution with 5000 independent trials at the fixed significance level 0.01.

⁶ All triangle meshes of the presented examples store $50 \cdot 100 = 5000$ unique vertices (with associated unit normals, colors and texture coordinates) and $2 \cdot (50 - 1) \cdot (100 - 1) = 9702$ triangular faces. Instead of rough approximations, the unit normals are calculated by normalizing the vector products of the calculated first order partial derivatives. During each mesh generation we used the default color scheme `TensorProductSurface3::DEFAULT_NULL_FRAGMENT`. Note that, in practice, usually it would be sufficient to generate triangle meshes with significantly less number of attributes and faces.

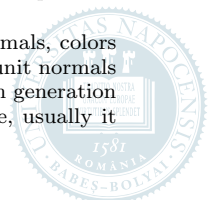


Table 2: Run-time statistics of examples presented in Section 2

Figure	Task	Run-time related confidence intervals ⁵
3(a)	Creating a B-surface object of minimal order and calculating the transformation matrices for the B-representation of the patch $\mathbf{s} _{[\frac{11\pi}{2}, \frac{49\pi}{8}] \times [-\frac{\pi}{3}, \frac{\pi}{3}]}$ of the ordinary exponential-trigonometric integral surface (30).	$(0.033229, 0.11037)_{\text{CPU}_1}$ $(0.083522, 0.11440)_{\text{CPU}_2}$
	Calculating the control net for the B-representation of the given patch and updating the vertex buffer object of the obtained control net.	$(0.00000, 0.03861)_{\text{CPU}_1}$ $(0.01892, 0.03412)_{\text{CPU}_2}$
	Generating its triangle mesh and updating the vertex buffer objects of the obtained mesh. ⁶	$(47.3069, 48.0527)_{\text{CPU}_1}$ $(24.6402, 25.5222)_{\text{CPU}_2}$
3(b)	Performing order elevation and updating the vertex buffer object of the order elevated control net. (More details can be found in Example 2.3.)	$(0.08402, 0.19038)_{\text{CPU}_1}$ $(0.16458, 0.20607)_{\text{CPU}_2}$
	Generating the triangle mesh of the order elevated B-surface and updating the vertex buffer objects of the obtained mesh.	$(70.3128, 71.1488)_{\text{CPU}_1}$ $(36.5207, 37.3169)_{\text{CPU}_2}$
3(c)	Performing order elevation and updating the vertex buffer object of the order elevated control net. (More details can be found in Example 2.3.)	$(0.32332, 0.50668)_{\text{CPU}_1}$ $(0.39463, 0.45833)_{\text{CPU}_2}$
	Generating the triangle mesh of the order elevated B-surface and updating its vertex buffer objects.	$(99.6233, 100.582)_{\text{CPU}_1}$ $(52.1324, 53.1988)_{\text{CPU}_2}$
4	Creating four B-surfaces and updating the vertex buffer objects of their control nets, by subdividing the initial surface patch $\mathbf{s} _{[\frac{11\pi}{2}, \frac{49\pi}{8}] \times [-\frac{\pi}{3}, \frac{\pi}{3}]}$ at the parameter value $u_1 = 0$, then by subdividing one of the obtained B-surface elements at the parameter value $u_0 = \frac{93\pi}{16}$.	$(0.46939, 0.69221)_{\text{CPU}_1}$ $(0.72089, 0.80915)_{\text{CPU}_2}$
	Generating the triangle meshes of the obtained B-surfaces and updating their vertex buffer objects.	$(194.946, 196.301)_{\text{CPU}_1}$ $(101.882, 103.559)_{\text{CPU}_2}$
5(c)	Multi-threaded calculation of control nets and the sequential update of their vertex buffer objects for the B-representation of the ordinary integral surface (30) by generating a 5×5 matrix of exponential-trigonometric B-surface patches of order $(n_0 = 6, n_1 = 2)$ and common shape parameters $(\beta_0 - \alpha_0 = \frac{29\pi}{40}, \beta_1 - \alpha_1 = \frac{2\pi}{5})$.	$(0.817715, 1.09069)_{\text{CPU}_1}$ $(0.729526, 1.03447)_{\text{CPU}_2}$
	Multi-threaded generation of each of the 25 triangle meshes of the obtained B-surface patches, then the sequential update of their vertex buffer objects.	$(1242.90, 1250.62)_{\text{CPU}_1}$ $(669.218, 678.874)_{\text{CPU}_2}$
17	Multi-threaded generation and first order differentiation of $5 \cdot 5 \cdot 5 \cdot 3 = 375$ isoparametric lines of Fig. 17, then updating their vertex buffer objects.	$(30.3413, 30.8631)_{\text{CPU}_1}$ $(19.6889, 20.5075)_{\text{CPU}_2}$

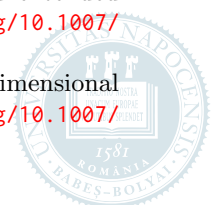
tools. Apart from some image post-processing (like adding L^AT_EX-like labels and other descriptive elements), all curve or surface illustrating figures were generated by means of the proposed function library which is not merely the collage implementation of already existing theoretical or numerical methods. Although some parts of our implementation rely on [1, 19], in Section 2 we have also formulated new original results in Theorems 2.1, 2.2, 2.3, 2.5 and 2.7. To the best of our knowledge, such a unifying general framework for curve and surface modeling was not presented in the literature so far. Even special cases of non-negative normalized B-bases (like the well-known Bernstein polynomials and their application possibilities) are considered to be important [24].

We have also included our detailed user manual [21] in the supplementary material of the manuscript that covers full implementation details and source code listings, by using which one is able both to reproduce all presented examples and to create new types of EC spaces, B-curves and B-surfaces in just a few lines of code. The user manual consists of three chapters. The first one provides a theoretical introduction without the proofs of the current Section 2. Labels and formulas of this chapter are used to clarify the full implementation details included in the second chapter of the user manual. Assuming that users provide an OpenGL based class that is able to create a rendering context and to handle possible events, the third chapter of the user manual concentrates on the constructor and rendering method of the aforementioned class in order to interactively manipulate different types of B-curves/surfaces, to perform operations (like order elevation and subdivision) on them and to provide B-representations for ordinary integral curves/surfaces.

We believe, the proposed library will help the development of other software packages for a large variety of real-world applications that arise from Approximation Theory, Computer Aided Geometric Design and Manufacturing, Computer Graphics, Isogeometric and Numerical Analysis.

References

1. J.-M. Carnicer, E. Mainar, and J. M. Peña. 2004. Critical length for design purposes and extended Chebyshev spaces. *Constructive Approximation* 20, 1 (2004), 55–71. DOI:<http://dx.doi.org/10.1007/s00365-002-0530-1>
2. J.-M. Carnicer, E. Mainar, and J. M. Peña. 2007. Shape preservation regions for six-dimensional spaces. *Advances in Computational Mathematics* 26, 1–3 (2007), 121–136. DOI:<http://dx.doi.org/10.1007/s10444-005-7505-2>



3. J.-M. Carnicer, E. Mainar, and J. M. Peña. 2014. On the critical length of cycloidal spaces. *Constructive Approximation* 39, 3 (2014), 573–583. DOI:<http://dx.doi.org/10.1007/s00365-013-9223-1>
4. J.-M. Carnicer and J. M. Peña. 1993. Shape preserving representations and optimality of the Bernstein basis. *Advances in Computational Mathematics* 1, 2 (1993), 173–196. DOI:<http://dx.doi.org/10.1007/BF02071384>
5. J.-M. Carnicer and J. M. Peña. 1994. Totally positive bases for shape preserving curve design and optimality of B-splines. *Computer Aided Geometric Design* 11, 6 (1994), 633–654. DOI:[http://dx.doi.org/10.1016/0167-8396\(94\)90056-6](http://dx.doi.org/10.1016/0167-8396(94)90056-6)
6. J.-M. Carnicer and J. M. Peña. 1995. On transforming a Tchebycheff system into a strictly totally positive system. *Journal of Approximation Theory* 81, 2 (1995), 274–295. DOI:<http://dx.doi.org/10.1006/jath.1995.1050>
7. P. Costantini, T. Lyche, and C. Manni. 2005. On a class of weak Tchebycheff systems. *Numer. Math.* 101, 2 (2005), 333–354. DOI:<http://dx.doi.org/10.1007/s00211-005-0613-6>
8. S. Karlin and W. Studden. 1966. *Tchebycheff systems: with applications in analysis and statistics*. Wiley, New York, NY.
9. Y. Lü, G. Wang, and X. Yang. 2002. Uniform hyperbolic polynomial B-spline curves. *Computer Aided Geometric Design* 19, 6 (2002), 379–393. DOI:[http://dx.doi.org/10.1016/S0167-8396\(02\)00092-4](http://dx.doi.org/10.1016/S0167-8396(02)00092-4)
10. T. Lyche. 1985. A recurrence relation for Chebyshevian B-splines. *Constructive Approximation* 1, 1 (1985), 155–173. DOI:<http://dx.doi.org/10.1007/BF01890028>
11. E. Mainar and J. M. Peña. 2004. Quadratic-cycloidal curves. *Advances in Computational Mathematics* 20, 1–3 (2004), 161–175. DOI:<http://dx.doi.org/10.1023/A:1025813919473>
12. E. Mainar and J. M. Peña. 2010. Optimal bases for a class of mixed spaces and their associated spline spaces. *Computers and Mathematics with Applications* 59, 4 (2010), 1509–1523. DOI:<http://dx.doi.org/10.1016/j.camwa.2009.11.009>
13. E. Mainar, J. M. Peña, and J. M. Sánchez-Reyes. 2001. Shape preserving alternatives to the rational Bézier model. *Computer Aided Geometric Design* 18, 1 (2001), 37–60. DOI:[http://dx.doi.org/10.1016/S0167-8396\(01\)00011-5](http://dx.doi.org/10.1016/S0167-8396(01)00011-5)
14. C. Manni, F. Pelosi, and M. L. Sampoli. 2011. Generalized B-splines as a tool in isogeometric analysis. *Computer Methods in Applied Mechanics and Engineering* 200, 5–8 (2011), 867–881. DOI:<http://dx.doi.org/10.1016/j.cma.2010.10.010>
15. M.-L. Mazure. 1999. Chebyshev–Bernstein bases. *Computer Aided Geometric Design* 16, 7 (1999), 649–669. DOI:[http://dx.doi.org/10.1016/S0167-8396\(99\)00029-1](http://dx.doi.org/10.1016/S0167-8396(99)00029-1)
16. M.-L. Mazure. 2001. Chebyshev splines beyond total positivity. *Advances in Computational Mathematics* 14, 2 (2001), 129–156. DOI:<http://dx.doi.org/10.1023/A:1016616731472>
17. J. M. Peña. 1999. *Shape Preserving Representations in Computer-Aided Geometric Design*. Nova Science Publishers, Commack, NY.
18. W. H. Press, S. A. Teukolsky, W. T. Vetterling, and B. P. Flannery. 2007. *Numerical Recipes 3rd Edition: The art of Scientific Computing*. Cambridge University Press, New York.
19. Á. Róth. 2015. Control point based exact description of curves and surfaces in extended Chebyshev spaces. *Computer Aided Geometric Design* 40 (2015), 40–58. DOI:<http://dx.doi.org/10.1016/j.cagd.2015.09.005>
20. Á. Róth. 2015. Control point based exact description of trigonometric/hyperbolic curves, surfaces and volumes. *J. Comput. Appl. Math.* 290, C (2015), 74–91. DOI:<http://dx.doi.org/10.1016/j.cam.2015.05.003>
21. Á. Róth. 2017. *User manual. An OpenGL and C++ based function library for curve and surface modeling in a large class of extended Chebyshev spaces* (1st ed.). Babeş–Bolyai University, Department of Mathematics and Informatics of the Hungarian Line, RO–400084 Cluj-Napoca, Romania. Supplementary material.
22. J. Sánchez-Reyes. 1998. Harmonic rational Bézier curves, p-Bézier curves and trigonometric polynomials. *Computer Aided Geometric Design* 15, 9 (1998), 909–923. DOI:[http://dx.doi.org/10.1016/S0167-8396\(98\)00031-4](http://dx.doi.org/10.1016/S0167-8396(98)00031-4)
23. W.-Q. Shen and G.-Z. Wang. 2005. A class of quasi Bézier curves based on hyperbolic polynomials. *Journal of Zhejiang University SCIENCE* 6A (Suppl. I), 9 (2005), 116–123. DOI:<http://dx.doi.org/10.1007/BF02887226>
24. Y.-F. Tsai and R. T. Farouki. 2001. Algorithm 812: BPOLY: An object-oriented library of numerical algorithms for polynomials in Bernstein form. *ACM Trans. Math. Software* 27, 2 (2001), 267–296. DOI:<http://dx.doi.org/10.1145/383738.383743>

